Higgs Spectroscopy of Superconductors

A new method to identify the superconducting gap symmetry

by

Nathan Cheng

B.Sc., The University of British Columbia, 2016

A THESIS SUBMITTED IN PARTIAL FULFILLMENT OF
THE REQUIREMENTS FOR THE DEGREE OF

MASTER OF SCIENCE

in

The Faculty of Graduate and Postdoctoral Studies

(Physics)

THE UNIVERSITY OF BRITISH COLUMBIA

(Vancouver)

August 2018

Committee Page

The following individuals certify that they have read, and recommend to the Faculty of Graduate and Postdoctoral Studies for acceptance, the thesis entitled:

Title: Higgs Spectroscopy of Superconductors

submitted by Nathan Cheng in partial fulfillment of the requirements for
the degree of Master of Science
in Physics

Examining Committee

Mona Berciu
Supervisor

Andrea Damascelli
Additional Examiner

Abstract

In this thesis we study the response of a BCS superconductor to an external ultra-fast terahertz electromagnetic field, which we choose so as to mimic the setup in a pump-probe experiment.

We begin by considering an optical experimental setup and demonstrate that in an optical pump-probe experiment, the superconducting amplitude Higgs mode can be excited and measured with ultra-fast terahertz pump pulses. Moreover, for an anistropic d-wave superconductor, there are two Higgs mode, one at the usual 2Δ energy and one with a lower energy. The latter can be used to differentiate the d-wave symmetry from isotropic s-wave, by varying the polarization of the pump relative to the sample. For a linearly polarized pump with a vector potential aligned along a d-wave node we find only a single Higgs mode, while for a direction along an antinode we find two Higgs modes.

Next, we consider an angle resolved photoemission spectroscopy (ARPES) experiment and derive a new set of equations of motion, for which we can analyze the two-time nonequilibrium Green's functions. We show that the Higgs mode can also be studied in an ARPES pump-probe experiment. Moreover, we show how an ARPES pump-probe experiment can be used to differentiate between different momentum-dependent nonequilibrium Higgs modes. Our results suggest that in a d-wave superconductor, the second low-energy Higgs mode is of osculating, B1g character, which corresponds to a symmetry breaking along the d-wave nodal lines. Further study of the role of momentum symmetry breaking promises to provide deeper insight into generating new nonequilibrium states.

Lay Summary

In this thesis, we develop a theoretical framework that can be used to elucidate future experimental findings in terahertz time-resolved experiments on superconductors. The theoretical framework and experimental methods proposed in this thesis can be used to characterize different symmetries inherent to superconductors in equilibrium and nonequilibrium. These advances in the field of Higgs spectroscopy promise to provide a deeper insight into superconducting dynamics and advance the growing field surrounding nonequilibrium superconductors and materials research.

Preface

- A version of the work discussed in Chapter 2 is currently published as *B. Fauseweh, L. Schwarz, N. Tsuji, N. Cheng, N. Bittner, H. Krull, M. Berciu, G. S. Uhrig, A. P. Schnyder, S. Kaiser, D. Manske* arXiv:1712.07989. It makes use of the formalism by Papenkort, Axt and Kuhn [37].
- I carried out the numerical calculations and numerical analysis in this publication, which pertain to the interaction of the superconductor with an electromagnetic field, while the analytic work on quenches and different nonequilibrium symmetries was primarily contributed by B. Fauseweh, L. Schwarz. and N. Tsuji. The project was primarily overseen by D. Manske and the publication is based on collaboration with Bittner, Krull, Berciu, Uhrig, Schnyder, Kaiser. The draft of the manuscript was also written by B. Fauseweh.
- I have also carried out all of the work in Chapter 3, which will be submitted for publication shortly.

Table of Contents

Appendices

List of Tables

List of Figures

Acknowledgements

I am so grateful to both Dirk Manske and Mona Berciu – Dirk for our ongoing collaboration, which has both opened up the world of physics to me as well as an entire new world of cultures, which I am very happy to now take part in. Your continuing advice, not just about physics, has been invaluable.

Mona Berciu has been above and beyond and I am so thankful to have had the opportunity to work with her. To me, she has been exceptionally kind, helpful and inspiring. Her dependable, calm reassurance has been a huge buoy to my entire MSc. experience. I am extremely thankful to her for her guidance.

The entirety of Mona Berciu's group has been extremely helpful to me – especially Stepan Fomichev, Mirko Möller and John Sous, whom I have had countless exceptional discussions with. I am also grateful to James Charbonneau, whose class I have had the pleasure of being a part of as a teaching assistant. Being a part of teaching has been one of my most valued parts of my Msc. Lastly, I am very thankful to Tim Jaschek, for our many scientific and unscientific discussions. His ongoing friendship has truly made my MSc. memorable.

I would like to thank all my friends who have made the past years an unforgettable experience and finally, my parents, Mark and Elizabeth, and my sister, Kira, whose love and encouragement has been my anchor.

Dedication

For my sister, whose wisdom creates such richness of life for all those around her.

Chapter 1

Introduction

Superconductivity, discovered in 1911 by Kamerlingh Onnes [51], continues to be one of the most interesting phases of matter. Originally shown to appear in mercury below 4.2 Kelvin, it is now known that most elemental metals and simple metallic compounds undergo a phase transition to a superconducting state below some critical temperature in the range of up to 20 K. Remarkably, upon cooling below this transition temperature, these materials exhibit absolutely zero resistivity and, partly as a consequence, expel weak magnetic fields from the bulk – the Meissner effect. As would later be discovered, the source of such peculiar properties is a low energy bosonic condensate with an energy gap corresponding to the condensate energy. However, this explanation would not be established until 45 years later.

These compounds became known as conventional superconductors when in 1986 the first so-called unconventional superconductor [7] was discovered in lanthanum doped copper oxide. Quickly, an entire class of copper oxide superconductors were discovered that continue to be an ongoing and challenging research topic in condensed matter physics. This class of superconductors is unique for a number of reasons, the first being an unusually high superconducting transition temperature. Among other peculiarities, these superconductors do not have a uniform superconducting energy gap. In fact, for certain points in the Brillouin zone, the superconducting gap actually closes. Since, there have been many other classes of superconductors with unconventional forms of momentum dependence beyond conventional s-wave – d-wave, s+/-, etc. – making symmetry a meaningful method of distinguishing between these classes.

1.1 BCS theory of superconductivity

As a testament to the difficulty of both experimentally probing and theoretically describing this phase, a microscopic description of conventional superconductivity was not discovered until the 1957 Bardeen Cooper and Schrieffer (BCS) theory of superconductivity [1–3, 11], for which they would receive the 1972 Nobel prize in physics (for unconventional superconductivity, a conclusive microscopic description remains elusive). While widely known in the 50s that a weak attractive potential can bind a pair of particles in two-dimensions, but not three, Cooper showed that certain three-dimensional electrons, which exist in a thin shell of energy near the Fermi energy (the Fermi surface) and in the presence of an attractive electron-electron potential, will also form pairs of bound states (Cooper pairs) between electrons of opposite momentum [11]. Together with Schrieffer and Bardeen, Cooper wrote down a microscopic Hamiltonian for such an interaction, which would become known as the BCS theory of superconductivity [2, 3]:

$$H_{BCS} = \sum_{\mathbf{k},\sigma} \epsilon_{\mathbf{k}} c^{\dagger}_{\mathbf{k},\sigma} c_{\mathbf{k},\sigma} + \sum_{\mathbf{k},\mathbf{k}'} \mathrm{V}_{\mathbf{k},\mathbf{k}'} c^{\dagger}_{\mathbf{k}\uparrow} c^{\dagger}_{-\mathbf{k}\downarrow} c_{-\mathbf{k}'\downarrow} c_{\mathbf{k}'\uparrow} \tag{1.1}$$

In the original work, the form of the potential $V_{\mathbf{k},\mathbf{k}'}$ was taken to be some constant attractive term between electrons (holes) $c^\dagger_{\mathbf{k},\sigma}$ ($c_{\mathbf{k},\sigma}$) of opposite spin and momentum in some band $\epsilon_{\mathbf{k}}$. However, the exact potential is now known to be highly momentum dependent depending on the specific superconductor. For instance, in the d-wave superconductors, the potential has a d-wave dependence, which we will discuss in detail below.

1.1.1 Mean-field superconductivity

Fortunately, for conventional superconductors in particular, electron pairs often span tens or even hundreds of lattice sites. As such, the electron (hole) pairing density is relatively constant and a mean-field approximation is well justified. Making such an approximation reduces the quartic superconducting Hamiltonian to a simple, quadratic Hamiltonian for a single particle and additionally defines a complex order parameter representing the superconducting gap $\Delta_{\mathbf{k}}$, which is defined in terms of the mean-field parameter,

$$\Delta_{\mathbf{k}'} = \sum_{\mathbf{k}\in\mathcal{W}} V_{\mathbf{k},\mathbf{k}'}\langle c_{-\mathbf{k}\downarrow}c_{\mathbf{k}\uparrow}\rangle. \tag{1.2}$$

Here, we also enforce the requirement that these electrons (holes) reside within a thin shell $\mathcal{W}$ above (below) the Fermi surface – as required for electrons (holes) to experience an attractive electron-electron (hole-hole) interaction. In this case, the mean-field Hamiltonian reduces to

$$H_{MF} = \sum_{\mathbf{k},\sigma} \epsilon_{\mathbf{k}} c^\dagger_{\mathbf{k},\sigma} c_{\mathbf{k},\sigma} + \sum_{\mathbf{k}\in\mathcal{W}} \Big[\Delta_{\mathbf{k}} c^\dagger_{\mathbf{k}\uparrow} c^\dagger_{-\mathbf{k}\downarrow} + \Delta^*_{\mathbf{k}} c_{-\mathbf{k}\downarrow} c_{\mathbf{k}\uparrow}\Big]. \tag{1.3}$$

It is convenient to write the Hamiltonian in terms of Bogoliubov quasiparticle operators, which are given by,

$$\alpha_{\mathbf{k}} = u^*_{\mathbf{k}} c_{\mathbf{k},\uparrow} + v_{\mathbf{k}} c^\dagger_{-\mathbf{k}\downarrow} \tag{1.4a}$$
$$\beta_{\mathbf{k}} = u^*_{\mathbf{k}} c_{-\mathbf{k}\downarrow} - v_{\mathbf{k}} c^\dagger_{\mathbf{k}\uparrow} \tag{1.4b}$$

Under these transformations and normalizing – $|u_{\mathbf{k}}|^2 + |v_{\mathbf{k}}|^2 = 1$ – the mean-field Hamiltonian written in terms of the Bogoliubov quasiparticles is then,

$$H_{MF} = \sum_{\mathbf{k}} \Big[R_{\mathbf{k}}\alpha^\dagger_{\mathbf{k}}\alpha_{\mathbf{k}} - R_{\mathbf{k}}\beta_{\mathbf{k}}\beta^\dagger_{\mathbf{k}} + C_{\mathbf{k}}\alpha^\dagger_{\mathbf{k}}\beta^\dagger_{\mathbf{k}} + C^*_{\mathbf{k}}\beta_{\mathbf{k}}\alpha_{\mathbf{k}}\Big] \tag{1.5}$$

where $R_{\mathbf{k}}$ and $C_{\mathbf{k}}$ are given by,

$$R_{\mathbf{k}} = \epsilon_{\mathbf{k}}(1 - 2v_{\mathbf{k}}v^*_{\mathbf{k}}) + \Delta^*_{\mathbf{k}} u_{\mathbf{k}} v_{\mathbf{k}} + \Delta u^*_{\mathbf{k}} v^*_{\mathbf{k}} \tag{1.6a}$$
$$C_{\mathbf{k}} = -2\epsilon_{\mathbf{k}} u^*_{\mathbf{k}} v_{\mathbf{k}} + \Delta_{\mathbf{k}}(u^*_{\mathbf{k}})^2 - \Delta^*_{\mathbf{k}}(v_{\mathbf{k}})^2 \tag{1.6b}$$

For finite $\Delta_{\mathbf{k}}$, the quasiparticle energy $E_{\mathbf{k}} = \sqrt{\epsilon^2_{\mathbf{k}} + |\Delta_{\mathbf{k}}|^2}$ is non-vanishing for all points around the Fermi surface, so the quasiparticle spectrum is gapped by $\Delta_{\mathbf{k}}$. As the superconducting gap $\Delta_{\mathbf{k}}$ closes to zero, $C_{\mathbf{k}}$ must vanish so that the Hamiltonian becomes diagonal; $R_{\mathbf{k}}$ then simply has the form of the band energy. We choose our normalization in such a way that $u_{\mathbf{k}}$ is real and $v_{\mathbf{k}}$ is complex and

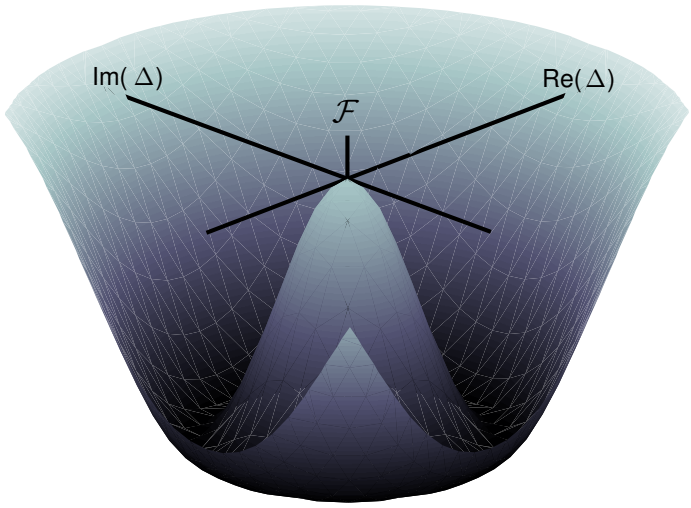

Figure 1.1: Ginzburg-Landau free energy potential in the superconducting phase with respect to some global order parameter Δ.

carries the phase of the gap, $\Delta_{\mathbf{k}}$. To satisfy these condition and re-obtain our original mean-field Hamiltonian $u_{\mathbf{k}}$ and $v_{\mathbf{k}}$ are defined in the following way:

$$u_{\mathbf{k}} = \sqrt{\frac{1}{2}\left(1 + \frac{\epsilon_{\mathbf{k}}}{E_{\mathbf{k}}}\right)} \tag{1.7a}$$

$$v_{\mathbf{k}} = \frac{\Delta_{\mathbf{k}}}{|\Delta_{\mathbf{k}}|}\sqrt{\frac{1}{2}\left(1 - \frac{\epsilon_{\mathbf{k}}}{E_{\mathbf{k}}}\right)} \tag{1.7b}$$

with $E_{\mathbf{k}} = \sqrt{\epsilon_{\mathbf{k}}^2 + |\Delta_{\mathbf{k}}|^2}$. Besides being of a much simpler form, this mean-field Hamiltonian also allowed the reconciliation of the BCS, microscopic theory of superconductivity with the more macroscopic or phenomenological, Ginzburg-Landau theory of superconductivity.

1.2 Ginzburg-Landau theory

Originally formulated prior to the BCS theory, the Ginzburg-Landau theory [18, 28] attempted to describe the continuous phase transition between the superconducting and normal states in terms of some global order parameter for which they gave no microscopic justification. Even so, their theory was rather effectively able to describe certain macroscopic properties according to this complex order parameter field. For instance, it allows one to derive two length-scales corresponding to the London penetration depth of a magnetic field into the superconductor and the characteristic length scale of superconducting density fluctuations, the superconducting coherence length. Ginzburg-Landau theory has since been derived beginning from the microscopic BCS description of superconductivity. In essence, Ginzburg-Landau theory is just an extension of Landau mean-field theory for continuous,

second order phase transitions. It states that in the absence of a superconducting current, the free energy density in the superconducting state, F_s, is the sum of the normal state free energy density F_n and terms depending on some complex field Δ (which we know from BCS theory corresponds to the superconducting order parameter).

$$F_s = F_n + \alpha|\Delta|^2 + \frac{\beta}{2}|\Delta|^4 \tag{1.8}$$

The total free energy is of course,

$$\mathscr{F} = \int dV F_s \tag{1.9}$$

Above the transition temperature T_c, this problem admits the trivial solution $|\Delta| = 0$ as a minimum solution for $\alpha > 0$. However for $\alpha < 0$ and $\beta > 0$, this problem admits a second solution for temperatures below T_c of the form,

$$|\Delta|^2 = -\frac{\alpha(T_c - T)}{\beta} \tag{1.10}$$

where the form of the temperature dependence of $\alpha = \alpha(T_c - T)$ below the transition temperature is included. The approximate form of α and β can also be derived from BCS theory for various thermodynamic points. This family of solutions corresponds to a nonzero minimum of $\mathscr{F}$ occurring exactly at $|\Delta|$ and, since the phase of Δ remains arbitrary, the free energy $\mathscr{F}$ has the form of the so-called "Mexican-hat" potential (Fig. 1.1).

1.3 Nonequilibrium spectroscopy

Researchers have always been interested in studying the dynamics of systems. Historically, such research led to the invention of the first motion picture films in the 1890s, which implemented shutter speeds on fast enough timescales to resolve and photograph the constituents of motion. To the same effect, nonequilibrium research in science has sought to capture the time-evolution of a variety of systems ranging from the flutter of a hummingbird's wings all the way down to the microscopic scale motion of atoms and electrons; the latter become increasingly more difficult to image as they require "shutter-speeds" fast enough to capture motion at the femtosecond and even shorter timescales. Among numerous nonequilibrium milestones, the 1967 Nobel Prize in Chemistry was awarded to Eigen, Norrish and Porter for the visualization of rapid chemical reactions and, with the development of femtosecond spectroscopy, the 1999 Nobel Prize in Chemistry was awarded to Zewail for his work on imaging transition states in chemical reactions. Modern time-resolved experiments operate across a wide spectrum of energies in the femtosecond and even attosecond timescale and are rapidly becoming more proficient in the study of quantum effects.

While the study of equilibrium properties may provide the foundations needed to describe a material, investigating its dynamics is crucial to developing a complete understanding [10, 13, 23, 33]. For instance, nonequilibrium experiments can access and probe non-thermal excited states otherwise inaccessible in thermal equilibrium. One of the most prominent tools to excite and study a system in nonequilibrium conditions is pump-probe spectroscopy. A pump pulse is first used to excite the system into a nonequilibrium state and after a short time delay, an ultra-fast probe pulse is used to measure the nonequilibrium state as a function of the delay time. Successive probes in turn can be

used to illustrate the time-resolved dynamics of the nonequilibrium state.

The profile of the pump used to excite the system can be varied to induce different excitation spectra. For instance, a continuous pumping pulse can be used to coherently excite a specific state, thereby providing a degree of optical control. Other optical pumps effectively excite the sample into a high temperature state, from which information can be deduced by studying the decay and the lifetime of the different induced excitations. However, both of these methods can be classified as adiabatic methods, as the relevant timescales are often much longer than the response time of the system. For the rest of this thesis, we will focus on non-adiabatic pump pulses, which occur on timescales faster than the response time of the system. Effectively, the pump acts as a quantum quench, driving the system into a nearby state while simultaneously inducing non-adiabatic excitations such as the Higgs amplitude mode. As a result, the effects are often highly non-linear and become increasingly difficult to study theoretically – especially in the field of strongly-correlated materials, which are already difficult to model, even in equilibrium.

1.4 Synopsis

An equilibrium superconducting condensate satisfies the minimum of Eq.1.8 by definition. In the following chapters we will theoretically investigate the nonequilibrium effects of perturbing the condensate and thus, the form of Eq. 1.8. We refer to this experimental technique as "Higgs spectroscopy". To study and characterize the resulting phenomena – the Higgs amplitude mode – we have developed software to solve the equations which follow, as well as a new formalism to describe the superconducting dynamics in time-resolved angle resolved photoemission spectroscopy (tr-ARPES) experiments. The thesis is outlined as follows.

In Chapter 2, we begin with an introduction to the nonequilibrium Ginzburg-Landau free energy picture of a superconductor. Following a brief introduction to the symmetries of the systems we wish to study – s-wave and d-wave – we derive the equations of motion for a BCS superconductor interacting with an electromagnetic field according to the standard density matrix formalism. We use this form of Hamiltonian and subsequent equations to mimic the form of a pump-probe experiment and compare the effects of exciting the Higgs amplitude mode(s) in s-wave and d-wave superconductors. We also calculate the relevant linear response functions for an optical experiment and predict possible techniques which can be used to experimentally measure these nonequilibrium modes. Our results reveal the possibility of exciting two out of the four Higgs amplitude modes in a d-wave superconductor. This is in contrast to an isotropic s-wave superconductor where only a single Higgs mode can be excited; there is only one nonequilibrium Higgs mode in an isotropic superconductor. Therefore, differentiating the Higgs amplitude mode excitations in a superconductor is a highly effective way of directly characterizing the condensate pairing symmetry.

To better understand the nature of the nonequilibrium modes, in Chapter 3 we derive a new formalism to calculate the two-time nonequilibrium Green's functions, which can be compared with tr-ARPES spectra. We show that, as in the case of time-resolved optical experiments, tr-ARPES can also be used to detect and distinguish s-wave and d-wave superconductors based on their Higgs amplitude mode response. Moreover, the ARPES momentum resolution can also be used to distinguish the symmetry of the nonequilibrium Higgs mode that is excited. For a linearly polarized pump incident on a d-wave superconductor, our results predict that aligning the magnetic potential

along a d-wave antinode will excite both the Higgs breathing mode (A1g) and Higgs osculating mode (B1g), while aligning the magnetic potential along a d-wave node will only excite the Higgs breathing mode. Lastly, we discuss a possible explanation and extensions for exciting other Higgs amplitude modes using the symmetry breaking of the linear electromagnetic pumping term.

Finally, in Chapter 4, we summarize the main results of this thesis and discuss further promising avenues to study superconductors via Higgs spectroscopy.

Chapter 2

Nonequilibrium Superconductivity: Optical Response

2.1 Introduction and analogy with Ginzburg-Landau theory

In this thesis we theoretically study the nature of a non-equilibrium superconductor that is excited and measured using pump-probe spectroscopy. Specifically, since we want to study rather low energy features, we will be interested primarily in energies in the range of a few terahertz, timescales on the order of a few hundred femptoseconds and small enough fluence that the superconducting state remains intact – the pump should not heat the superconductor into the normal state. Considering the narrow experimental window, these experiments are difficult and come close to the boundary of allowable experimental precision given by the Heisenberg uncertainty principle. However, recent experiments have been successful in studying non-equilibrium isotropic superconductors [29–32] and have just begun studying anisotropic superconductors [24], thus paving the way towards directly probing the superconducting condensate. A myriad of theoretical proposals and experiments have been conducted [4–6, 8, 9, 15, 16, 25–27, 34–50, 52, 53] to study phenomena ranging from coupled superconductors to other exotic phenomena. In this thesis, we develop a theoretical framework to prove that experimental measurements of the Higgs amplitude mode can uncover the superconducting symmetry, thus laying the foundation for studying these phenomena via the new technique of "Higgs spectroscopy".

Let us return to the Mexican hat potential, which coincidentally, also arises in high energy physics with the Higgs boson. Since a Cooper pair is in fact a boson, a superconductor can be viewed as a condensed matter analogue to the high-energy physics Higgs-boson [22]. This equivalency of structure gives rise to the nomenclature of the Higgs amplitude mode. For a superconducting condensate at the minimum of the potential, there are clearly two oscillatory modes permitted – an amplitude Higgs mode up and down the walls of the potential and a Goldstone phase mode around the minimum of the Mexican hat (Fig. 2.1).

To experimentally investigate the Higgs mode, pump-probe spectroscopy must be employed to induce and measure the non-equilibrium state. Physically, a few pairs of electrons are broken by the pumping pulse, which causes the Mexican-hat potential to shrink slightly, but does not destroy the overall superconductivity. As the potential is altered, one of two scenarios can occur. Either the potential is shrunk slowly so that the condensate is only excited in an adiabatic fashion and always remains at the bottom of the potential, or the potential is shrunk faster than the condensate can respond. In this latter non-adiabatic case, the condensate will wind up elevated above the new potential minimum along the potential wall. This intermediary state then relaxes towards the new equilibrium, giving rise to the Higgs oscillations.

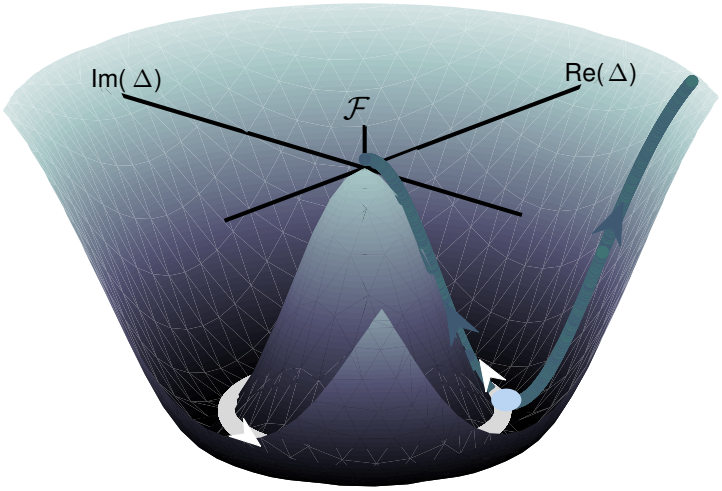

Figure 2.1: Nonequilibrium superconducting oscillatory modes. The amplitude Higgs mode manifests as the condensate oscillates up and down the potential walls (green line). The Goldstone mode manifests as the condensate phase oscillates around the potential minimum (white line).

2.1.1 Superconducting symmetries

Superconductors are different from high-energy physics models in that they also allow further degrees of freedom – the momentum dependence of the superconducting order parameter and the symmetry of the lattice. In this sense, superconductors actually host an additional degree of freedom through which one can probe the Higgs mode [4, 39, 41]. One of the key results of this work will be to investigate the effect of including the momentum dependence on the Higgs amplitude mode and discovering a second Higgs mode for certain anisotropic momentum dependencies.

In this thesis, we work solely with a two-dimensional square lattice. In this case, the two superconducting symmetries, s and $d_{x^2-y^2}$, belong to the $A1g$ and $B1g$ representations of the D_4 point group (Table 2.1) because they are even (odd) under C_4 rotation around the z-axis out of plane, even (even) under C_2' rotation around the x and y axes intersecting the antinodes and even (odd) under C_2'' rotation around the $\hat{xy}$ axis intersecting the nodes [14]. While in an isotropic superconductor, the nonequilibrium Higgs only permits a single mode – A1g isotropic expansion and contraction of the order parameter – as momentum anisotropy is introduced, the superconductor can permit various nonequilibrium Higgs oscillations depending on the specific group symmetries of the order parameter and the lattice. For instance, a $d_{x^2-y^2}$ superconductor can admit four possible in-plane nonequilibrium amplitude modes corresponding to the A1g, A2g, B1g and B2g symmetries listed in Table 2.1 and illustrated pictorially in Fig. 2.2. The focus of this thesis will be on studying differences between the most common superconducting symmetries, s and $d_{x^2-y^2}$, though the predictions and analysis can easily be extended to other symmetries using group theory considerations.

D_4 Table	E	C_2	$2C_4$	$2C_2'$	$2C_2''$
A_{1g}	1	1	1	1	1
A_{2g}	1	1	1	-1	-1
B_{1g}	1	1	-1	1	-1
B_{2g}	1	1	-1	-1	1

Table 2.1: Character table for the D_4 point group. For a square lattice aligned along the x and y axes, C_2 and C_4 correspond to rotations about the z-axis. C_2' corresponds to rotations around the x and y axes. C_2'' corresponds to rotations around the xy-axes.

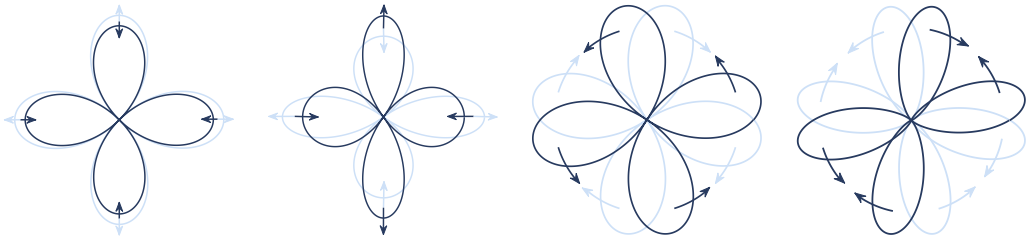

(a) Breathing mode (b) Osculating mode (c) Rotating mode (d) Clapping mode

Figure 2.2: Pictorial representation of all four possible $d_{x^2-y^2}$ nonequilibrium Higgs amplitude modes, as allowed by group symmetry considerations. In terms of the group symmetry they are the (a) A1g breathing mode, (b) B1g osculating mode, (c) A2g rotating mode, (d) B2g clapping mode.

2.2 Model Hamiltonian

We now consider a time-dependent Hamiltonian. In particular, we study the time-evolution of a BCS superconductor in the presence of some time-varying electromagnetic potential, which will take the form of a realistic experimental pumping or probing laser. As a starting point, a mean-field BCS superconductor H_{MF} is considered together with some electromagnetic interaction H_{EM}. This will prove to be an auspicious starting point, as many experimental techniques probe such light-matter material interactions. We are especially interested in the class of pump-probe experiments that probe the time-dependence of particular properties following some electromagnetic pump excitation, which disturbs the equilibrium of the material. The Hamiltonian is,

$$H = H_{MF} + H_{EM}^{(1)} + H_{EM}^{(2)} \tag{2.1}$$

where we have broken up the electromagnetic interaction term into linear and quadratic order terms. Following the discussion from the previous chapter, the BCS mean-field Hamiltonian is given by,

$$H_{MF} = \sum_{\mathbf{k},\sigma} \epsilon_{\mathbf{k}} c^\dagger_{\mathbf{k},\sigma} c_{\mathbf{k},\sigma} + \sum_{\mathbf{k}\in\mathcal{W}} \Big[\Delta_{\mathbf{k}} c^\dagger_{\mathbf{k}\uparrow} c^\dagger_{-\mathbf{k}\downarrow} + \Delta^*_{\mathbf{k}} c_{-\mathbf{k}\downarrow} c_{\mathbf{k}\uparrow}\Big]. \tag{2.2}$$

where $c^\dagger_{\mathbf{k},\sigma}$ and $c_{\mathbf{k},\sigma}$ are, respectively, the electron creation and annihilation operators for an electron of momentum $\mathbf{k}$ and spin σ. $\epsilon_{\mathbf{k}} = \hbar^2\mathbf{k}^2/(2m) - E_F$ is the electron dispersion for a single quadratic band with a circular Fermi surface, m is the effective mass and E_F is the Fermi energy level. $\mathcal{W}$ is the set of all momentum vectors $\mathbf{k}$, such that $|\epsilon_{\mathbf{k}}| \leq \hbar\omega_c$ for some cutoff energy $\hbar\omega_c$ in the pairing interaction. Finally, Δ is the mean-field gap-parameter determined by the microscopic interaction $V_{\mathbf{k},\mathbf{k}'}$

$$\Delta_{\mathbf{k}'} = \sum_{\mathbf{k}\in\mathcal{W}} V_{\mathbf{k},\mathbf{k}'} \langle c_{-\mathbf{k}\downarrow} c_{\mathbf{k}\uparrow}\rangle. \tag{2.3}$$

The electromagnetic portion of the Hamiltonian in second quantization is,

$$H_{EM}^{(1)} = \frac{e\hbar}{2m} \sum_{\mathbf{k},\mathbf{q},\sigma} (2\mathbf{k}+\mathbf{q}) \cdot \mathbf{A}_{\mathbf{q}}(t) c^\dagger_{\mathbf{k}+\mathbf{q},\sigma} c_{\mathbf{k}\sigma} \tag{2.4a}$$

$$H_{EM}^{(2)} = \frac{e^2}{2m} \sum_{\mathbf{k},\mathbf{q},\sigma} \left[\sum_{\mathbf{q}'} \mathbf{A}_{\mathbf{q}-\mathbf{q}'}(t) \cdot \mathbf{A}_{\mathbf{q}'}(t)\right] c^\dagger_{\mathbf{k}+\mathbf{q},\sigma} c_{\mathbf{k}\sigma} \tag{2.4b}$$

where $\mathbf{A}_{\mathbf{q}}$ is the electromagnetic vector potential for a momentum transfer $\mathbf{q}$.

We now make a change of basis to Bogoliubov quasiparticle operators, which are again given in Eq. 1.4. This change of basis will be more intuitive when we consider the time-dependent equations of motion for the superconductor. Under this change of basis, the mean-field superconducting Hamiltonian (Eq. 2.2) becomes,

$$H_{MF} = \sum_{\mathbf{k}} \Big[R_{\mathbf{k}} \alpha^\dagger_{\mathbf{k}} \alpha_{\mathbf{k}} - R_{\mathbf{k}} \beta_{\mathbf{k}} \beta^\dagger_{\mathbf{k}} + C_{\mathbf{k}} \alpha^\dagger_{\mathbf{k}} \beta^\dagger_{\mathbf{k}} + C^*_{\mathbf{k}} \beta_{\mathbf{k}} \alpha_{\mathbf{k}}\Big] \tag{2.5}$$

where $R_{\mathbf{k}}$ and $C_{\mathbf{k}}$ are the same as in Eq. 1.6. We now also need to make the change of basis for the electromagnetic term H_{EM}.

$$H_{EM}^{(1)} = \frac{e\hbar}{2m}\sum_{\mathbf{k},\mathbf{q}}(2\mathbf{k}+\mathbf{q})\cdot\mathbf{A}_{\mathbf{q}}(\mathbf{t})\Big[(u^*_{\mathbf{k+q}}u_{\mathbf{k}} + v_{\mathbf{k+q}}v^*_{\mathbf{k}})\alpha^\dagger_{\mathbf{k+q}}\alpha_{\mathbf{k}} - (v^*_{\mathbf{k+q}}v_{\mathbf{k}} + u^*_{\mathbf{k}}u_{\mathbf{k+q}})\beta^\dagger_{\mathbf{k}}\beta_{\mathbf{k+q}}$$
$$+(v_{\mathbf{k+q}}u^*_{\mathbf{k}} - u^*_{\mathbf{k+q}}v_{\mathbf{k}})\alpha^\dagger_{\mathbf{k+q}}\beta^\dagger_{\mathbf{k}} + (v^*_{\mathbf{k}}u_{\mathbf{k+q}} - v^*_{\mathbf{k+q}}u_{\mathbf{k}})\beta_{\mathbf{k+q}}\alpha_{\mathbf{k}}\Big] \tag{2.6a}$$

$$H_{EM}^{(2)} = \frac{e^2}{2m}\sum_{\mathbf{k},\mathbf{q}}\left(\sum_{\mathbf{q}'}\mathbf{A}_{\mathbf{q}-\mathbf{q}'}(t)\cdot\mathbf{A}_{\mathbf{q}'}(t)\right)\Big[(u^*_{\mathbf{k+q}}u_{\mathbf{k}} - v_{\mathbf{k+q}}v^*_{\mathbf{k}})\alpha^\dagger_{\mathbf{k+q}}\alpha_{\mathbf{k}} - (v^*_{\mathbf{k+q}}v_{\mathbf{k}} - u^*_{\mathbf{k}}u_{\mathbf{k+q}})\beta^\dagger_{\mathbf{k}}\beta_{\mathbf{k+q}}$$
$$-(v_{\mathbf{k+q}}u^*_{\mathbf{k}} + u^*_{\mathbf{k+q}}v_{\mathbf{k}})\alpha^\dagger_{\mathbf{k+q}}\beta^\dagger_{\mathbf{k}} - (v^*_{\mathbf{k}}u_{\mathbf{k+q}} + v^*_{\mathbf{k+q}}u_{\mathbf{k}})\beta_{\mathbf{k+q}}\alpha_{\mathbf{k}}\Big] \tag{2.6b}$$

Though the phase in a superconductor is arbitrary, we can fix a specific initial phase of Δ for our calculations. In fact, we have verified that varying this initial choice of phase has no impact on the calculation beyond the initial phase-offset. Therefore, to simplify notation, we choose our initial Δ to be real and positive and employ the following shorthand for the subsequent sections,

$$\begin{aligned} L^{\pm}_{\mathbf{k},\mathbf{q}} &= u_{\mathbf{k+q}}u_{\mathbf{k}} \pm v_{\mathbf{k+q}}v_{\mathbf{k}} \\ M^{\pm}_{\mathbf{k},\mathbf{q}} &= u_{\mathbf{k+q}}v_{\mathbf{k}} \pm v_{\mathbf{k+q}}u_{\mathbf{k}} \end{aligned} \tag{2.7}$$

2.3 Equations of motion

To calculate the time-dependence of various quantities in the system, there are generally two different approaches. One can take the quasiparticle operators to be time-dependent and the states themselves to be time-independent (the Heisenberg picture), or the quasiparticle states to be time-dependent and the operators time-independent (the Schrödinger picture). We will utilize the first approach, which involves solving the Heisenberg equations of motion for an operator $\hat{A}$,

$$\frac{d}{dt}\hat{A}(t) = \frac{i}{\hbar}[H,\hat{A}(t)] + \left(\frac{\partial\hat{A}}{\partial t}\right)_H \tag{2.8}$$

Since our interest is in determining experimental observables, our choice of working in the Heisenberg picture makes taking any expectation value with respect to our time-independent states trivial. The particular values we will be interested in are the four quasiparticle expectation values that appear in our Hamiltonian with various momenta: $\langle\alpha^\dagger_{\mathbf{k}}\alpha_{\mathbf{k+q}}\rangle(t)$, $\langle\beta^\dagger_{\mathbf{k}}\beta_{\mathbf{k+q}}\rangle(t)$, $\langle\alpha^\dagger_{\mathbf{k}}\beta^\dagger_{\mathbf{k+q}}\rangle(t)$ and $\langle\alpha_{\mathbf{k}}\beta_{\mathbf{k+q}}\rangle(t)$. The α and β operators are intrinsically time-independent. Therefore, for these expectation values, the last term in Eq. 2.8 will be identically zero. The Heisenberg equations of motion we need to

solve are:

$$i\hbar\frac{d}{dt}\langle\alpha^\dagger_{\mathbf{k}}\beta^\dagger_{\mathbf{k+q}}\rangle = -\left\langle\left[H,\alpha^\dagger_{\mathbf{k}}\beta^\dagger_{\mathbf{k+q}}\right]\right\rangle = -\left\langle\left[H_{sc}+H^{(1)}_{em}+H^{(2)}_{em},\alpha^\dagger_{\mathbf{k}}\beta^\dagger_{\mathbf{k+q}}\right]\right\rangle, \tag{2.9a}$$

$$i\hbar\frac{d}{dt}\langle\alpha_{\mathbf{k}}\beta_{\mathbf{k+q}}\rangle = -\langle[H,\alpha_{\mathbf{k}}\beta_{\mathbf{k+q}}]\rangle = -\left\langle\left[H_{sc}+H^{(1)}_{em}+H^{(2)}_{em},\alpha_{\mathbf{k}}\beta_{\mathbf{k+q}}\right]\right\rangle, \tag{2.9b}$$

$$i\hbar\frac{d}{dt}\langle\alpha^\dagger_{\mathbf{k}}\alpha_{\mathbf{k+q}}\rangle = -\left\langle\left[H,\alpha^\dagger_{\mathbf{k}}\alpha_{\mathbf{k+q}}\right]\right\rangle = -\left\langle\left[H_{sc}+H^{(1)}_{em}+H^{(2)}_{em},\alpha^\dagger_{\mathbf{k}}\alpha_{\mathbf{k+q}}\right]\right\rangle, \tag{2.9c}$$

$$i\hbar\frac{d}{dt}\langle\beta^\dagger_{\mathbf{k}}\beta_{\mathbf{k+q}}\rangle = -\left\langle\left[H,\beta^\dagger_{\mathbf{k}}\beta_{\mathbf{k+q}}\right]\right\rangle = -\left\langle\left[H_{sc}+H^{(1)}_{em}+H^{(2)}_{em},\beta^\dagger_{\mathbf{k}}\beta_{\mathbf{k+q}}\right]\right\rangle \tag{2.9d}$$

If we return to our Hamiltonian, this means that the order parameter describing the system will incur an explicit time-dependence. Rewriting $\Delta(t)$ in terms of Bogoliubov quasiparticle expectation values, we find

$$\Delta_{\mathbf{k}'}(t) = \sum_{\mathbf{k}\in\mathcal{W}} V_{\mathbf{k},\mathbf{k}'}\left[u_{\mathbf{k}}v_{\mathbf{k}}(\langle\alpha^\dagger_{\mathbf{k}}\alpha_{\mathbf{k}}\rangle(t)+\langle\beta^\dagger_{\mathbf{k}}\beta_{\mathbf{k}}\rangle(t)-1)-u^2_{\mathbf{k}}\langle\alpha_{\mathbf{k}}\beta_{\mathbf{k}}\rangle(t)-v^2_{\mathbf{k}}\langle\alpha^\dagger_{\mathbf{k}}\beta^\dagger_{\mathbf{k}'}\rangle(t)\right] \tag{2.10}$$

where the explicit time-dependence has been included for all of the constituents.

2.3.1 Equations of motion following the pump

Before we proceed with the explicit calculation, it is convenient to choose a specific electromagnetic field profile, which can help to simplify the number of equations we need to solve. The particular choice we make for the electromagnetic field, which will constitute the pumping laser in a pump-probe experiment, is a classical monochromatic laser source – an electromagnetic field with a single well-defined frequency and momentum. The exact time-dependent profile need not be fixed, however we choose a Gaussian shape, which should be representative of most experimental setups. We define the vector potential for the pump, $\mathbf{A}_{\mathbf{q}}(t)$,

$$\mathbf{A}_{\mathbf{q}}(t) = \mathbf{A}_{\mathrm{p}}\,\exp\left[-\left(\frac{2\sqrt{\ln 2}t}{\tau_p}\right)^2\right](\delta_{\mathbf{q},\mathbf{q}_0}e^{-i\omega_p t}+\delta_{\mathbf{q},-\mathbf{q}_0}e^{i\omega_p t}) \tag{2.11}$$

where the amplitude of the pump is $\mathbf{A}_p$ and the full width at half maximum is τ_p. The pumping frequency and momentum are given by ω_p and $\mathbf{q_p}$. We also choose a linear polarization for $\mathbf{A_p}$ such that the momentum vector $\mathbf{q}_p$ and the vector potential $\mathbf{A}_{\mathbf{q}}(t)$ are orthogonal vectors as required by electromagnetic theory.

Taking the commutator with the Hamiltonian, the time-dependent equations of motion for our four quasiparticle expectation values are given by:

$$
\begin{aligned}
i\hbar\frac{d}{dt}\langle\alpha^\dagger_{\mathbf{k}}\beta^\dagger_{\mathbf{k}'}\rangle = &-(R_{\mathbf{k}}+R_{\mathbf{k}'})\langle\alpha^\dagger_{\mathbf{k}}\beta^\dagger_{\mathbf{k}'}\rangle + C^*_{\mathbf{k}'}\langle\alpha^\dagger_{\mathbf{k}}\alpha_{\mathbf{k}'}\rangle + C^*_{\mathbf{k}}(\langle\beta^\dagger_{\mathbf{k}'}\beta_{\mathbf{k}}\rangle - \delta_{\mathbf{k}',\mathbf{k}}) \\
&+\frac{e\hbar}{2m}\sum_{\mathbf{q}'=\pm\mathbf{q}_0} 2\mathbf{k}\cdot\mathbf{A}_{\mathbf{q}'}(t)\Big[-L^+_{\mathbf{k},\mathbf{q}'}\langle\alpha^\dagger_{\mathbf{k}+\mathbf{q}'}\beta^\dagger_{\mathbf{k}'}\rangle + L^+_{\mathbf{k}',-\mathbf{q}'}\langle\alpha^\dagger_{\mathbf{k}}\beta^\dagger_{\mathbf{k}'-\mathbf{q}'}\rangle \\
&\qquad -M^-_{\mathbf{k}'-\mathbf{q}'}\langle\alpha^\dagger_{\mathbf{k}}\alpha_{\mathbf{k}'-\mathbf{q}'}\rangle + M^-_{\mathbf{k},\mathbf{q}'}(\langle\beta^\dagger_{\mathbf{k}'}\beta_{\mathbf{k}+\mathbf{q}'}\rangle - \delta_{\mathbf{k}'-\mathbf{k},\mathbf{q}'})\Big] \\
&+\frac{e^2}{2m}\sum_{\mathbf{q}'=0,\pm2\mathbf{q}_0}\sum_{\mathbf{q}_i=\pm\mathbf{q}_0}\mathbf{A}_{\mathbf{q}'-\mathbf{q}_i}(t)\cdot\mathbf{A}_{\mathbf{q}_i}(t)\Big[-L^-_{\mathbf{k},\mathbf{q}'}\langle\alpha^\dagger_{\mathbf{k}+\mathbf{q}'}\beta^\dagger_{\mathbf{k}'}\rangle - L^-_{\mathbf{k}',-\mathbf{q}'}\langle\alpha^\dagger_{\mathbf{k}}\beta^\dagger_{\mathbf{k}'-\mathbf{q}'}\rangle \\
&\qquad -M^+_{\mathbf{k}'-\mathbf{q}'}\langle\alpha^\dagger_{\mathbf{k}}\alpha_{\mathbf{k}'-\mathbf{q}'}\rangle + M^+_{\mathbf{k},\mathbf{q}'}(-\langle\beta^\dagger_{\mathbf{k}'}\beta_{\mathbf{k}+\mathbf{q}'}\rangle + \delta_{\mathbf{k}'-\mathbf{k},\mathbf{q}'})\Big]
\end{aligned}
\tag{2.12}
$$

$$
\begin{aligned}
i\hbar\frac{d}{dt}\langle\alpha_{\mathbf{k}}\beta_{\mathbf{k}'}\rangle = &+(R_{\mathbf{k}}+R_{\mathbf{k}'})\langle\alpha_{\mathbf{k}}\beta_{\mathbf{k}'}\rangle + C_{\mathbf{k}'}\langle\alpha^\dagger_{\mathbf{k}'}\alpha_{\mathbf{k}}\rangle + C_{\mathbf{k}}(\langle\beta^\dagger_{\mathbf{k}}\beta_{\mathbf{k}'}\rangle - \delta_{\mathbf{k}',\mathbf{k}}) \\
&+\frac{e\hbar}{2m}\sum_{\mathbf{q}'=\pm\mathbf{q}_0} 2\mathbf{k}\cdot\mathbf{A}_{\mathbf{q}'}(t)\Big[+L^{+*}_{\mathbf{k},\mathbf{q}'}\langle\alpha_{\mathbf{k}+\mathbf{q}'}\beta_{\mathbf{k}'}\rangle - L^{+*}_{\mathbf{k}',-\mathbf{q}'}\langle\alpha_{\mathbf{k}}\beta_{\mathbf{k}'-\mathbf{q}'}\rangle \\
&\qquad -M^{-*}_{\mathbf{k}'-\mathbf{q}'}\langle\alpha^\dagger_{\mathbf{k}'-\mathbf{q}'}\alpha_{\mathbf{k}}\rangle + M^{-*}_{\mathbf{k},\mathbf{q}'}(\langle\beta^\dagger_{\mathbf{k}+\mathbf{q}'}\beta_{\mathbf{k}}\rangle - \delta_{\mathbf{k}'-\mathbf{k},\mathbf{q}'})\Big] \\
&+\frac{e^2}{2m}\sum_{\mathbf{q}'=0,\pm2\mathbf{q}_0}\sum_{\mathbf{q}_i=\pm\mathbf{q}_0}\mathbf{A}_{\mathbf{q}'-\mathbf{q}_i}(t)\cdot\mathbf{A}_{\mathbf{q}_i}(t)\Big[+L^{-*}_{\mathbf{k},\mathbf{q}'}\langle\alpha_{\mathbf{k}+\mathbf{q}'}\beta_{\mathbf{k}'}\rangle + L^{+*}_{\mathbf{k}',-\mathbf{q}'}\langle\alpha_{\mathbf{k}}\beta_{\mathbf{k}'-\mathbf{q}'}\rangle \\
&\qquad -M^{+*}_{\mathbf{k}'-\mathbf{q}'}\langle\alpha^\dagger_{\mathbf{k}'-\mathbf{q}'}\alpha_{\mathbf{k}}\rangle + M^{+*}_{\mathbf{k},\mathbf{q}'}(-\langle\beta^\dagger_{\mathbf{k}+\mathbf{q}'}\beta_{\mathbf{k}}\rangle + \delta_{\mathbf{k}'-\mathbf{k},\mathbf{q}'})\Big]
\end{aligned}
\tag{2.13}
$$

$$
\begin{aligned}
i\hbar\frac{d}{dt}\langle\alpha^\dagger_{\mathbf{k}}\alpha_{\mathbf{k}'}\rangle = &+(R_{\mathbf{k}'}-R_{\mathbf{k}})\langle\alpha^\dagger_{\mathbf{k}}\alpha_{\mathbf{k}'}\rangle + C_{\mathbf{k}'}\langle\alpha^\dagger_{\mathbf{k}}\beta^\dagger_{\mathbf{k}'}\rangle + C^*_{\mathbf{k}}\langle\alpha_{\mathbf{k}'}\beta_{\mathbf{k}}\rangle \\
&+\frac{e\hbar}{2m}\sum_{\mathbf{q}'=\pm\mathbf{q}_0} 2\mathbf{k}\cdot\mathbf{A}_{\mathbf{q}'}(t)\Big[-L^+_{\mathbf{k},\mathbf{q}'}\langle\alpha^\dagger_{\mathbf{k}+\mathbf{q}'}\alpha_{\mathbf{k}'}\rangle + L^{+*}_{\mathbf{k}',-\mathbf{q}'}\langle\alpha^\dagger_{\mathbf{k}}\alpha_{\mathbf{k}'-\mathbf{q}'}\rangle \\
&\qquad +M^-_{\mathbf{k},\mathbf{q}'}\langle\alpha_{\mathbf{k}'}\beta_{\mathbf{k}+\mathbf{q}'}\rangle + M^{-*}_{\mathbf{k}',-\mathbf{q}'}\langle\alpha^\dagger_{\mathbf{k}}\beta^\dagger_{\mathbf{k}'+\mathbf{q}'}\rangle\Big] \\
&+\frac{e^2}{2m}\sum_{\mathbf{q}'=0,\pm2\mathbf{q}_0}\sum_{\mathbf{q}_i=\pm\mathbf{q}_0}\mathbf{A}_{\mathbf{q}'-\mathbf{q}_i}(t)\cdot\mathbf{A}_{\mathbf{q}_i}(t)\Big[-L^-_{\mathbf{k},\mathbf{q}'}\langle\alpha^\dagger_{\mathbf{k}+\mathbf{q}'}\alpha_{\mathbf{k}'}\rangle + L^{-*}_{\mathbf{k}',-\mathbf{q}'}\langle\alpha^\dagger_{\mathbf{k}}\alpha_{\mathbf{k}'-\mathbf{q}'}\rangle \\
&\qquad -M^+_{\mathbf{k},\mathbf{q}'}\langle\alpha_{\mathbf{k}'}\beta_{\mathbf{k}+\mathbf{q}'}\rangle - M^{+*}_{\mathbf{k}',-\mathbf{q}'}\langle\alpha^\dagger_{\mathbf{k}}\beta^\dagger_{\mathbf{k}'+\mathbf{q}'}\rangle\Big]
\end{aligned}
\tag{2.14}
$$

$$
\begin{aligned}
i\hbar\frac{d}{dt}\langle\beta^\dagger_{\mathbf{k}}\beta_{\mathbf{k}'}\rangle = &+(R_{\mathbf{k}'}-R_{\mathbf{k}})\langle\beta^\dagger_{\mathbf{k}}\beta_{\mathbf{k}'}\rangle + C_{\mathbf{k}'}\langle\alpha^\dagger_{\mathbf{k}}\beta^\dagger_{\mathbf{k}'}\rangle + C^*_{\mathbf{k}}\langle\alpha_{\mathbf{k}'}\beta_{\mathbf{k}}\rangle \\
&+\frac{e\hbar}{2m}\sum_{\mathbf{q}'=\pm\mathbf{q}_0} 2\mathbf{k}\cdot\mathbf{A}_{\mathbf{q}'}(t)\Big[+L^+_{\mathbf{k},-\mathbf{q}'}\langle\beta^\dagger_{\mathbf{k}-\mathbf{q}'}\beta_{\mathbf{k}'}\rangle - L^{+*}_{\mathbf{k}',\mathbf{q}'}\langle\beta^\dagger_{\mathbf{k}}\beta_{\mathbf{k}'+\mathbf{q}'}\rangle \\
&\qquad -M^-_{\mathbf{k},\mathbf{q}'}\langle\alpha_{\mathbf{k}'}\beta_{\mathbf{k}+\mathbf{q}'}\rangle - M^{-*}_{\mathbf{k}',-\mathbf{q}'}\langle\alpha^\dagger_{\mathbf{k}}\beta^\dagger_{\mathbf{k}'+\mathbf{q}'}\rangle\Big] \\
&+\frac{e^2}{2m}\sum_{\mathbf{q}'=0,\pm2\mathbf{q}_0}\sum_{\mathbf{q}_i=\pm\mathbf{q}_0}\mathbf{A}_{\mathbf{q}'-\mathbf{q}_i}(t)\cdot\mathbf{A}_{\mathbf{q}_i}(t)\Big[-L^-_{\mathbf{k},-\mathbf{q}'}\langle\beta^\dagger_{\mathbf{k}-\mathbf{q}'}\beta_{\mathbf{k}'}\rangle + L^{-*}_{\mathbf{k}',\mathbf{q}'}\langle\beta^\dagger_{\mathbf{k}}\beta_{\mathbf{k}'+\mathbf{q}'}\rangle \\
&\qquad -M^{+*}_{\mathbf{k}',\mathbf{q}'}\langle\alpha^\dagger_{\mathbf{k}'+\mathbf{q}'}\beta^\dagger_{\mathbf{k}}\rangle - M^+_{\mathbf{k},-\mathbf{q}'}\langle\alpha_{\mathbf{k}-\mathbf{q}'}\beta_{\mathbf{k}'}\rangle\Big]
\end{aligned}
\tag{2.15}
$$

After integrating these differential equations, one can determine the pump induced changes in the superconducting order parameter and by extension, the amplitude mode Higgs oscillations, via Eq. 2.10.

2.3.2 Equations of motion following the probe

Next, we want to consider the equations of motion following a second probing pulse, which will measure experimental observables. In particular, we are interested in the optical response, which can be related to the current density induced by the probe, $\mathbf{j}_{\mathbf{q}_{\mathrm{pr}}}$. Again we split up the response into two parts,

$$\mathbf{j}_{-\mathbf{q}_{\mathrm{pr}}} = \mathbf{j}^{(1)}_{-\mathbf{q}_{\mathrm{pr}}} + \mathbf{j}^{(2)}_{-\mathbf{q}_{\mathrm{pr}}} \tag{2.16a}$$

$$\mathbf{j}^{(1)}_{-\mathbf{q}_{\mathrm{pr}}} = \frac{-e\hbar}{2mV}\sum_{\mathbf{k},\sigma}(2\mathbf{k}+\mathbf{q}_{\mathrm{pr}})c^\dagger_{\mathbf{k},\sigma}c_{\mathbf{k}+\mathbf{q}_{\mathrm{pr}},\sigma} \tag{2.16b}$$

$$\mathbf{j}^{(2)}_{-\mathbf{q}_{\mathrm{pr}}} = -\frac{e^2}{mV}\sum_{\mathbf{k},\mathbf{q},\sigma}\mathbf{A}_{\mathbf{q}_{\mathrm{pr}}-\mathbf{q}}c^\dagger_{\mathbf{k},\sigma}c_{\mathbf{k}+\mathbf{q}_{\mathrm{pr}},\sigma} \tag{2.16c}$$

where V is the normalization volume. The second term $\mathbf{j}^{(2)}_{\mathbf{q}_{\mathrm{pr}}}$, is the diamagnetic current density, which has previously been shown [37, 38] to only lead to an offset in the imaginary part of the spectrum and therefore may be neglected. Performing the same transformation to the Bogoliubov quasiparticle basis, the current density $\mathbf{j}^{(1)}_{\mathbf{q}_{\mathrm{pr}}}$ is given by,

$$
\begin{aligned}
\mathbf{j}^{(1)}_{-\mathbf{q}_{\mathrm{pr}}} = \frac{-e\hbar}{2mV}\sum_{\mathbf{k}}(2\mathbf{k}+\mathbf{q}_{\mathrm{pr}})\Big[&(u^*_{\mathbf{k}}u_{\mathbf{k}+\mathbf{q}_{\mathrm{pr}}}+v_{\mathbf{k}}v^*_{\mathbf{k}+\mathbf{q}_{\mathrm{pr}}})\alpha^\dagger_{\mathbf{k}}\alpha_{\mathbf{k}+\mathbf{q}_{\mathrm{pr}}} - (v^*_{\mathbf{k}}v_{\mathbf{k}+\mathbf{q}_{\mathrm{pr}}}+u^*_{\mathbf{k}+\mathbf{q}_{\mathrm{pr}}}u_{\mathbf{k}})\beta^\dagger_{\mathbf{k}+\mathbf{q}_{\mathrm{pr}}}\beta_{\mathbf{k}} \\
&+(v_{\mathbf{k}}u^*_{\mathbf{k}+\mathbf{q}_{\mathrm{pr}}}-u^*_{\mathbf{k}}v_{\mathbf{k}+\mathbf{q}_{\mathrm{pr}}})\alpha^\dagger_{\mathbf{k}}\beta^\dagger_{\mathbf{k}+\mathbf{q}_{\mathrm{pr}}} + (v^*_{\mathbf{k}}u_{\mathbf{k}+\mathbf{q}_{\mathrm{pr}}}-v^*_{\mathbf{k}+\mathbf{q}_{\mathrm{pr}}}u_{\mathbf{k}})\alpha_{\mathbf{k}+\mathbf{q}_{\mathrm{pr}}}\beta_{\mathbf{k}}\Big]
\end{aligned}
\tag{2.17}
$$

With the current density, we can then calculate other quantities such as the optical conductivity σ,

$$\sigma(\omega) = \frac{\langle\mathbf{j}_{\mathbf{q}_{\mathrm{pr}}}\rangle(\omega)}{i\omega\mathbf{A}_{\mathbf{q}_{\mathrm{pr}}}(\omega)} \tag{2.18}$$

by taking the Fourier transform of $\mathbf{j}(t)$ and $\mathbf{A}_{\mathbf{q}_{\mathrm{pr}}}(t)$, where the probing vector potential takes the

same functional form as the pumping vector potential in Eq. 2.11. The exact parameters of the probe will differ from those used in the pump.

We now turn to the equations of motion following the probing pulse. As is the case with most optical experimental setups, we work with a probing pulse polarized perpendicular to the pumping pulse so that the off-diagonal terms are decoupled between the two pulses. To simplify this portion of the calculation, we assume that the probe pulse is sufficiently weak that it need only be calculated to linear order. Second, we assume that the prominent excitations are induced by the pump, so that we can approximate $\langle \alpha^\dagger_{\mathbf{k}+\mathbf{q}_{\rm pr}} \beta_{\mathbf{k}+\mathbf{q}_{\rm pr}} \rangle \simeq \langle \alpha^\dagger_{\mathbf{k}+\mathbf{q}_{\rm p}} \beta_{\mathbf{k}+\mathbf{q}_{\rm p}} \rangle$, where we have used the subscripts pr and p to represent the probe and pump respectively.

The differential equations for the expectation values of the quasiparticles needed to calculate the optical response of the probe are as follows:

$$\begin{aligned} i\hbar \frac{d}{dt} \langle \alpha^\dagger_{\mathbf{k}} \beta^\dagger_{\mathbf{k}+\mathbf{q}_{\rm pr}} \rangle = &-(R_{\mathbf{k}} + R_{\mathbf{k}+\mathbf{q}_{\rm pr}}) \langle \alpha^\dagger_{\mathbf{k}} \beta^\dagger_{\mathbf{k}+\mathbf{q}_{\rm pr}} \rangle + C^*_{\mathbf{k}+\mathbf{q}_{\rm pr}} \langle \alpha^\dagger_{\mathbf{k}} \alpha_{\mathbf{k}+\mathbf{q}_{\rm pr}} \rangle + C^*_{\mathbf{k}} \langle \beta^\dagger_{\mathbf{k}+\mathbf{q}_{\rm pr}} \beta_{\mathbf{k}} \rangle \\ &+ \frac{e\hbar}{2m} 2\mathbf{k} \cdot \mathbf{A}_{\mathbf{q}_{\rm pr}}(t) \Big[-L^+_{\mathbf{k},\mathbf{q}_{\rm pr}} \langle \alpha^\dagger_{\mathbf{k}+\mathbf{q}_{\rm p}} \beta^\dagger_{\mathbf{k}+\mathbf{q}_{\rm p}} \rangle + L^+_{\mathbf{k},\mathbf{q}_{\rm pr}} \langle \alpha^\dagger_{\mathbf{k}} \beta^\dagger_{\mathbf{k}} \rangle \\ &\quad + M^-_{\mathbf{k},\mathbf{q}_{\rm pr}} \langle \alpha^\dagger_{\mathbf{k}} \alpha_{\mathbf{k}} \rangle + M^-_{\mathbf{k},\mathbf{q}_{\rm pr}} (\langle \beta^\dagger_{\mathbf{k}+\mathbf{q}_{\rm p}} \beta_{\mathbf{k}+\mathbf{q}_{\rm p}} \rangle - 1) \Big] \end{aligned} \tag{2.19}$$

$$\begin{aligned} i\hbar \frac{d}{dt} \langle \alpha_{\mathbf{k}+\mathbf{q}_{\rm pr}} \beta_{\mathbf{k}} \rangle = &+(R_{\mathbf{k}} + R_{\mathbf{k}+\mathbf{q}_{\rm pr}}) \langle \alpha_{\mathbf{k}+\mathbf{q}_{\rm pr}} \beta_{\mathbf{k}} \rangle + C_{\mathbf{k}} \langle \alpha^\dagger_{\mathbf{k}} \alpha_{\mathbf{k}+\mathbf{q}_{\rm pr}} \rangle + C_{\mathbf{k}+\mathbf{q}_{\rm pr}} \langle \beta^\dagger_{\mathbf{k}+\mathbf{q}_{\rm pr}} \beta_{\mathbf{k}} \rangle \\ &+ \frac{e\hbar}{2m} 2\mathbf{k} \cdot \mathbf{A}_{\mathbf{q}_{\rm pr}}(t) \Big[+L^+_{\mathbf{k},\mathbf{q}_{\rm pr}} \langle \alpha_{\mathbf{k}} \beta_{\mathbf{k}} \rangle - L^+_{\mathbf{k},\mathbf{q}_{\rm pr}} \langle \alpha_{\mathbf{k}+\mathbf{q}_{\rm p}} \beta_{\mathbf{k}+\mathbf{q}_{\rm p}} \rangle \\ &\quad - M^-_{\mathbf{k},\mathbf{q}_{\rm pr}} \langle \alpha^\dagger_{\mathbf{k}+\mathbf{q}_{\rm pr}} \alpha_{\mathbf{k}+\mathbf{q}_{\rm pr}} \rangle - M^-_{\mathbf{k},\mathbf{q}_{\rm pr}} (\langle \beta^\dagger_{\mathbf{k}} \beta_{\mathbf{k}} \rangle - 1) \Big] \end{aligned} \tag{2.20}$$

$$\begin{aligned} i\hbar \frac{d}{dt} \langle \alpha^\dagger_{\mathbf{k}} \alpha_{\mathbf{k}+\mathbf{q}_{\rm pr}} \rangle = &-(R_{\mathbf{k}} - R_{\mathbf{k}+\mathbf{q}_{\rm pr}}) \langle \alpha^\dagger_{\mathbf{k}} \alpha_{\mathbf{k}+\mathbf{q}_{\rm pr}} \rangle + C_{\mathbf{k}+\mathbf{q}_{\rm pr}} \langle \alpha^\dagger_{\mathbf{k}} \beta^\dagger_{\mathbf{k}+\mathbf{q}_{\rm pr}} \rangle + C^*_{\mathbf{k}} \langle \alpha_{\mathbf{k}+\mathbf{q}_{\rm pr}} \beta_{\mathbf{k}} \rangle \\ &+ \frac{e\hbar}{2m} 2\mathbf{k} \cdot \mathbf{A}_{\mathbf{q}_{\rm pr}}(t) \Big[-L^+_{\mathbf{k},\mathbf{q}_{\rm pr}} \langle \alpha^\dagger_{\mathbf{k}+\mathbf{q}_{\rm p}} \alpha_{\mathbf{k}+\mathbf{q}_{\rm p}} \rangle + L^+_{\mathbf{k},\mathbf{q}_{\rm pr}} \langle \alpha^\dagger_{\mathbf{k}} \alpha_{\mathbf{k}} \rangle \\ &\quad + M^-_{\mathbf{k},\mathbf{q}_{\rm pr}} \langle \alpha_{\mathbf{k}+\mathbf{q}_{\rm p}} \beta_{\mathbf{k}+\mathbf{q}_{\rm p}} \rangle - M^-_{\mathbf{k},\mathbf{q}_{\rm pr}} \langle \alpha^\dagger_{\mathbf{k}} \beta^\dagger_{\mathbf{k}} \rangle \Big] \end{aligned} \tag{2.21}$$

$$\begin{aligned} i\hbar \frac{d}{dt} \langle \beta^\dagger_{\mathbf{k}+\mathbf{q}_{\rm pr}} \beta_{\mathbf{k}} \rangle = &+(R_{\mathbf{k}} - R_{\mathbf{k}+\mathbf{q}_{\rm pr}}) \langle \beta^\dagger_{\mathbf{k}+\mathbf{q}_{\rm pr}} \beta_{\mathbf{k}} \rangle + C_{\mathbf{k}} \langle \alpha^\dagger_{\mathbf{k}} \beta^\dagger_{\mathbf{k}+\mathbf{q}_{\rm pr}} \rangle + C^*_{\mathbf{k}+\mathbf{q}_{\rm pr}} \langle \alpha_{\mathbf{k}+\mathbf{q}_{\rm pr}} \beta_{\mathbf{k}} \rangle \\ &+ \frac{e\hbar}{2m} 2\mathbf{k} \cdot \mathbf{A}_{\mathbf{q}_{\rm pr}}(t) \Big[L^+_{\mathbf{k},\mathbf{q}_{\rm pr}} \langle \beta^\dagger_{\mathbf{k}} \beta_{\mathbf{k}} \rangle - L^+_{\mathbf{k},\mathbf{q}_{\rm pr}} \langle \beta^\dagger_{\mathbf{k}+\mathbf{q}_{\rm p}} \beta_{\mathbf{k}+\mathbf{q}_{\rm p}} \rangle \\ &\quad + M^-_{\mathbf{k},\mathbf{q}_{\rm pr}} \langle \alpha_{\mathbf{k}} \beta_{\mathbf{k}} \rangle - M^-_{\mathbf{k},\mathbf{q}_{\rm pr}} \langle \alpha^\dagger_{\mathbf{k}+\mathbf{q}_{\rm p}} \beta^\dagger_{\mathbf{k}+\mathbf{q}_{\rm p}} \rangle \Big] \end{aligned} \tag{2.22}$$

2.3.3 Initial conditions and numerical approximations

The Bogoliubov quasiparticles are fermions and obey Fermi statistics. Therefore, we can calculate the occupation values for a given temperature prior to the pump or probe pulse as follows,

$$\langle \alpha^\dagger_{\mathbf{k}} \alpha_{\mathbf{k}'} \rangle = \frac{1}{e^{\frac{E_{\mathbf{k}}}{k_B T}} + 1} \delta_{\mathbf{k},\mathbf{k}'} \tag{2.23a}$$

$$\langle \beta^\dagger_{\mathbf{k}} \beta_{\mathbf{k}'} \rangle = \frac{1}{e^{\frac{E_{\mathbf{k}}}{k_B T}} + 1} \delta_{\mathbf{k},\mathbf{k}'} \tag{2.23b}$$

$$\langle \alpha^\dagger_{\mathbf{k}} \beta^\dagger_{\mathbf{k}'} \rangle = 0 \tag{2.23c}$$

$$\langle \alpha_{\mathbf{k}} \beta_{\mathbf{k}'} \rangle = 0 \tag{2.23d}$$

where $E_{\mathbf{k}} = \sqrt{\epsilon_{\mathbf{k}} + \Delta_{\mathbf{k}}}$ is the quasiparticle energy. For our calculations, we limit ourselves to the $T = 0$ case. Qualitatively, the results are similar for sufficiently low temperatures.

Next, we choose the superconducting symmetries to consider. We primarily study the two well known superconductor symmetries: s-wave and d-wave. In this case, our interaction term in Eq. 2.10, $V_{\mathbf{k},\mathbf{k}'}$, is of the form

$$V_{\mathbf{k},\mathbf{k}'} = V \tag{2.24}$$

or

$$V_{\mathbf{k},\mathbf{k}'} = V(\cos k_x - \cos k_y)(\cos k'_x - \cos k'_y) \tag{2.25}$$

for s-wave and d-wave ($d_{x^2-y^2}$) respectively. However, it would be trivial to extend our formalism to other interaction symmetries in one and two-dimensions, such as p-wave.

We can now proceed to fix V, or Δ and the other superconducting properties. When choosing which type of pump and probe, the pumping timescale should be on the same scale as the response time of the superconductor, which turns out to be in the order of a few hundred femptoseconds for superconducting gaps in the order of a few meVs. As discussed previously, this is required to induce a non-adiabatic excitation such as the Higgs amplitude mode. The superconducting parameters used throughout this thesis were historically used to study a lead superconductor, however we have investigated the effects of varying superconducting parameters and for a reasonable choice of pump and probe pulses, the effects are purely quantitative and have do not change the qualitative results. Therefore, we proceed with the same parameters for both s-wave and d-wave for comparison. The exact values used in our calculation are presented in Table 2.2.

We also need to make certain choices to simplify the numerical calculations, so long as they do not affect the qualitative results of our calculations. We take a 2-D momentum grid with spacing along the pumping momentum direction equal to the pumping momentum transfer. This may seem unjustified at first, but our pumping momentum is extremely small (see Table 2.2) and we have also numerically verified that choosing a smaller discretization does not affect the calculation. In the second momentum direction, we choose to rather discretize the angle for simplicity. This turns out to being equivalent to choosing Chebyshev points along the second direction. Furthermore, this gives us the most equal distribution of points between nodes for the case of a d-wave superconductor. For the d-wave case, we approximate the pairing as $\Delta_k = \Delta_0 \cos 2\theta$. We also limit the number of off-diagonal terms to four. In Eq. 2.3.1, this amounts to restricting $|\mathbf{k} - \mathbf{k}'| < 5\mathbf{q_0}$. Lastly, the

Parameters					
Superconductor		Pump		Probe	
a	10^{-10} m	$\hbar\omega_{\rm p}$	3.0 meV	$\hbar\omega_{\rm pr}$	2.5 meV
E_F	9470 meV	$\omega_{\rm p}$	4.56×10^{-3} fs^{-1}	$\omega_{\rm pr}$	3.80×10^{-3} fs^{-1}
m	$1.9m_e$	$A_{\rm p}$	$7.0\times10^{-8}\frac{\rm J\ s}{\rm C\ m}$	$A_{\rm pr}$	$0.7\times10^{-8}\frac{\rm J\ s}{\rm C\ m}$
w_c	8.3 meV	$\tau_{\rm p}$	400 fs^{-1}	$\tau_{\rm pr}$	250.0 fs^{-1}
Δ_0	1.35 meV	$q_{\rm p}\ a$	1.52×10^{-6}	$q_{\rm pr}\ a$	1.26×10^{-6}

Table 2.2: Parameters for our calculations. a is the lattice spacing, E_F is the Fermi energy, m is the re-normalized mass and w_c is the cutoff frequency. Δ_0 is the initial size of the gap before the pump is turned on. $\omega_{p/pr}$, $A_{p/pr}$, $\tau_{p/pr}$ and $q_{p/pr}$ are the pump/probe frequency, amplitude, full width at half maximum and momentum.

standard fourth-order Runge-Kutta method is used to time-evolve the density matrices according to the equations of motion.

2.4 Results

2.4.1 Higgs oscillations

Following the application of a pumping laser, the magnitude of the order parameter decreases and oscillates due to changes in the free energy potential of the superconductor. The degree to which the potential is altered depends both on the amplitude and length of the pump. For longer duration and larger amplitudes, more Cooper pairs are depleted, which decreases the central value about which the order parameter oscillates. The strongest signal occurs for a pumping laser on the order of a few hundred femptoseconds, or faster than the intrinsic superconductor response time. Additionally, the amplitude or fluence of the pump should not be so large that the number of Cooper pairs is so significantly depleted that oscillations cannot occur.

The results for our specific parameters are presented in Fig. 2.3. At $t = 0$, the pump is turned on and the magnitude of the order parameter rapidly decreases as Cooper pairs are broken; the order parameter then begins to oscillate after the pump is turned off. In Fig. 2.3(a) , the Higgs oscillations of an isotropic, s-wave superconductor interacting with a laser are presented. As previously found for the case of an isotropic superconductor, ([37, 38], etc.) the oscillations decay with a characteristic $1/\sqrt{t}$ dephasing of the Bogoliubov quasiparticles and the oscillations themselves have a characteristic 2Δ frequency (Fig. 2.3(c)), where Δ is the new order parameter in the $t = \infty$ limit. Increasing the total amount of incident energy, will further decrease this value of the order parameter, as well as the frequency of the oscillations. These results are contrasted with the Higgs oscillations of a $d_{x^2-y^2}$ superconductor (Fig. 2.3(b)). Most notably, the $d_{x^2-y^2}$ superconductor oscillations depend strongly on the angle between the superconductor and polarization of the laser. $\phi = 0$ corresponds to a magnetic vector potential aligned along one of the $d_{x^2-y^2}$ antinodes (and subsequently, the

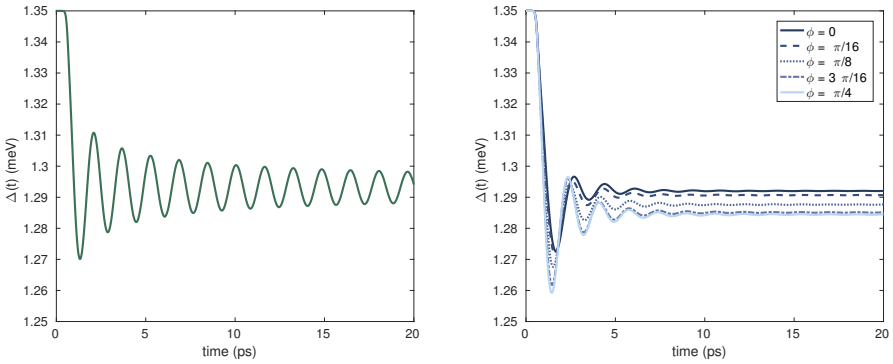

(a) s-wave (b) $d_{x^2-y^2}$

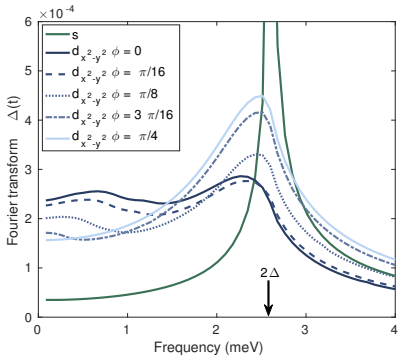

(c)

Figure 2.3: Comparison of s-wave (a) and d-wave (b) Higgs oscillations following the pumping pulse for the parameters given in Table 2.2. (c) Fourier transform of (a) and (b). ϕ is the relative angle between the vector potential and the $d_{x^2-y^2}$ antinode.

momentum vector also points perpendicularly along an adjacent node), while $\phi = \pi/4$ corresponds to having the vector potential aligned along one of the nodes. Moreover, the oscillations themselves are much smaller in amplitude and have a much more rapid decay, which has partly contributed to the difficulty thus far in detecting Higgs oscillations in anisotropic superconductors. The differences are perhaps best illustrated in the Fourier transform of the oscillations (Fig. 2.3(c)). While the isotropic, s-wave superconductor has a single sharp oscillation frequency at 2Δ, depending on the polarization angle ϕ, the $d_{x^2-y^2}$ superconductor has as many as 2 oscillation frequencies. As the polarization angle ϕ is rotated from the node to the antinode, the amplitude of the 2Δ mode decreases and a second mode develops below 2Δ. The frequency of this second mode also depends strongly on the amplitude and particularly the duration of the pump. The exact symmetry of this second mode will become more apparent in the following chapter.

2.4.2 Optical response

After the pump, a probing pulse is applied to measure the oscillations of the gap parameter $\Delta(t)$. In reality, many probing pulses are applied to measure the oscillation at various time-delays δt between

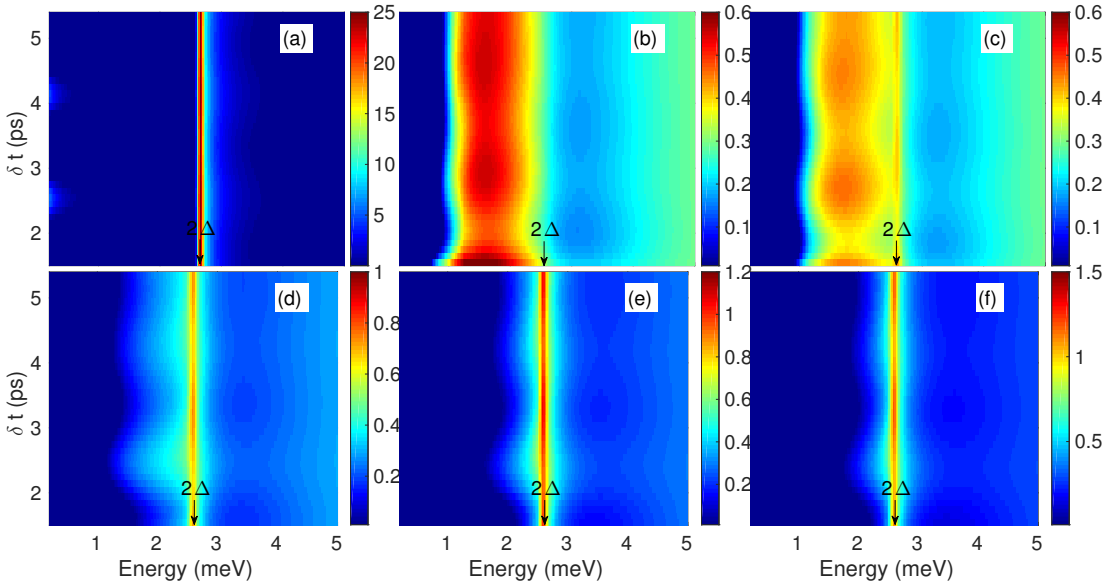

Figure 2.4: Comparison of different optical conductivity Higgs responses between (a) an s-wave superconductor and (b-f) a $d_{x^2-y^2}$ superconductor for the parameters in Table 2.2. The relative angle ϕ between the vector potential and the $d_{x^2-y^2}$ antinode is (b) $\phi = 0$ (c) $\phi = \pi/16$ (d) $\phi = \pi/8$ (e) $\phi = 3\pi/16$ (f) $\phi = \pi/4$.

the pump and the probe, each of which define a different set of differential equations to be solved. δt is a measure of the time-difference between the centers of the pump and probe pulses. For pump and probe time-scales on the order of a few hundred femptoseconds, this means that the smallest allowable time-delay, without significant pump and probe overlap, is around one picosecond.

The results for our parameters are presented in Fig. 2.4. For an isotropic s-wave superconductor (Fig. 2.4 (a)), there is clearly only a single, sharp mode in the conductivity spectra at 2Δ. The oscillation frequency in delay-time δt is also equal to 2Δ as expected from our analysis of the order parameter after the pump. In contrast, the conductivity response of a $d_{x^2-y^2}$ superconductor is very different. For a linear pump polarization such that the vector potential is aligned along the $d_{x^2-y^2}$ antinode ($\phi = 0$), there is a broad mode below 2Δ. The exact energy of the second mode depends on the specifics of the pump, but not on the geometry. As the vector potential of the pump is rotated towards the node (away from the anti-node), the intensity of the low energy mode decreases, while the intensity of the 2Δ mode increases until around an angle of $\pi/8$ between the vector potential and the d-wave anti-node, at which point the second mode is no longer visible in the conductivity spectra. The intensity of the 2Δ mode increases to a maximum when the vector potential and d-wave node become perfectly aligned ($\phi = \pi/4$). As for the oscillations in time-delay, they have both the frequencies of the 2Δ mode and the mode below 2Δ. Lastly, the signal has an eight-fold reflection symmetry as the pump polarization is rotated around the remaining $7\pi/4$ degrees; the signal is identical to the reflection across the $\pi/4$, C_2'' axis and the C_4' axis. In other words, there is no differentiation between positive and negative antinodes, nor is there a difference for points of equal amplitude across a single antinode.

2.5 Discussion

As we have shown, the Higgs amplitude mode of a nonequilibrium superconductor can be excited and measured in an optical pump-probe experiment with terahertz pumping energies and a pumping duration on the order of a few hundred femptoseconds. Moreover, the Higgs amplitude mode can be used to differentiate between isotropic and anisotropic superconductors, simply by rotating the sample relative to the polarization of the pump. For a $d_{x^2-y^2}$ superconductor, this corresponds to the excitation of an additional mode below the isotropic 2Δ mode as the vector potential is rotated to lie along an antinode. In an optical experiment, this can be detected either by noting the appearance of a low energy mode below the 2Δ energy or by observing changes to the frequency of the oscillations as a function of time-delay between the pump and probe. Our results also can easily be extended to different symmetries, for instance $s_\pm$ or p symmetries, which we expect will also be simple to differentiate from the two cases presented here, but will follow similar trends. Therefore, among other possibilities, exciting the Higgs amplitude mode via Higgs spectroscopy offers an unambiguous method for studying and differentiating between the different superconducting symmetries in a material.

What remains is to identify the specific symmetries of the nonequilibrium modes. While we expect the 2Δ mode in the $d_{x^2-y^2}$ superconductor to correspond to the isotropic breathing mode since this is the only possible mode for the isotropic s-wave superconductor, the mode below 2Δ in the $d_{x^2-y^2}$ superconductor is not quite as easy to identify using momentum integrated spectroscopy. We do not expect the nonequilibrium mode to acquire any angular momentum, therefore the osculating mode is the most likely candidate. However, this does not rule out the potential of generating these additional nonequilibrium modes by introducing additional pumping pulses of various geometries, which could produce the angular momentum necessary to generate other nonequilibrium modes. To determine the exact symmetry which is broken in this setup, it will be necessary to study the Higgs modes with momentum resolved spectroscopy, presented in the next chapter.

Chapter 3

Nonequilibrium Superconductivity: ARPES

3.1 Introduction to Green's functions

We turn now to the study of nonequilibrium superconductivity beyond the context of optical experiments. Namely, we want to study how the Higgs oscillation(s) will manifest in various other experimental contexts. In condensed matter physics, one of the most powerful tools for describing a system is the set of Green's functions, which are closely related to various experimental observables such as those measured in angle resolved photoemission spectroscopy (ARPES) [12, 13, 17] or scanning tunneling microscopy (STM). Since we will be working at zero temperature, only the zero-temperature Green's functions are presented. The two-time electron Green's function for a translationally invariant system is given by,

$$G_{\sigma,\sigma'}(\mathbf{k}',t,t') = -i\langle \mathscr{T} c_{\mathbf{k},\sigma}(t), c^\dagger_{\mathbf{k},\sigma'}(t')\rangle \tag{3.1}$$

where $\mathscr{T}$ is the time ordering operator and $c^\dagger_{\mathbf{k},\sigma}$ ($c_{\mathbf{k},\sigma}$) creates an electron (hole) with momentum $\mathbf{k}$ and spin σ. For the sake of simplicity and relevance to our problem, we only consider Green's functions for states of equal spin, since our Hamiltonian is spin symmetric. The Green's function is also closely related to four other quantities, the nonequilibrium greater and lesser Green's functions, $G^{\lessgtr}(\mathbf{k},t,t')$ and the retarded and advanced Green's functions, $G^R(\mathbf{k},t,t')$ and $G^A(\mathbf{k},t,t')$. They are defined as follows:

$$G^>(\mathbf{k}',t,t') = -i\langle c_{\mathbf{k},\sigma}(t), c^\dagger_{\mathbf{k},\sigma}(t')\rangle \tag{3.2a}$$
$$G^<(\mathbf{k}',t,t') = +i\langle c^\dagger_{\mathbf{k},\sigma}(t'), c_{\mathbf{k},\sigma}(t)\rangle \tag{3.2b}$$
$$G^R(\mathbf{k}',t,t') = -i\Theta(t-t')\langle \{c_{\mathbf{k},\sigma}(t), c^\dagger_{\mathbf{k},\sigma}(t')\}\rangle \tag{3.2c}$$
$$G^A(\mathbf{k}',t,t') = +i\Theta(t'-t)\langle \{c^\dagger_{\mathbf{k},\sigma}(t), c_{\mathbf{k},\sigma}(t')\}\rangle. \tag{3.2d}$$

In non-equilibrium photoemission spectroscopy, the ARPES intensity I_{ARPES}, is related to the spectral function, $A(\mathbf{k},\omega)$ of the non-equilibrium Green's function. Often, this is presented simply in terms of the lesser Green's function, $G^<(\mathbf{k},\omega)$, which gives us information about the electronic density (as opposed to information regarding the hole density, which is given by $G^>(\mathbf{k},\omega)$).

$$I_{ARPES} \propto \text{Im } G^<(\mathbf{k},\omega,\delta t) \tag{3.3}$$

where $G^<(\mathbf{k},\omega,\delta t)$ is the Fourier transform of $G^<(\mathbf{k},t'-t,\delta t)$ and δt is the time-difference between

the pump and the probe. The non-equilibrium spectral function also relates the retarded and advanced Green's functions to the lesser and greater Green's functions according to

$$A(\mathbf{k},t,t') = G^{>}(\mathbf{k},t,t') - G^{<}(\mathbf{k},t,t') = G^{R}(\mathbf{k},t,t') - G^{A}(\mathbf{k},t,t'). \tag{3.4}$$

Therefore, in order to study properties of the nonequilibrium ARPES signal, we must develop a formalism for evaluating the expectation value for two times rather than a single time as we have done previously.

3.2 Model Hamiltonian

Since we want to study the same phenomena and how it manifests in different experiments, we begin with the same Hamiltonian as in the previous chapter – a mean-field BCS superconductor placed in an arbitrary electromagnetic field.

$$H = H_{MF} + H_{EM}^{(1)} + H_{EM}^{(2)} \tag{3.5}$$

For clarity, the relevant equations for the Hamiltonian are presented again. In terms of the Bogoliubov quasiparticles,

$$\alpha_{\mathbf{k}} = u_{\mathbf{k}}^{*} c_{\mathbf{k},\uparrow} + v_{\mathbf{k}} c_{-\mathbf{k}\downarrow}^{\dagger} \tag{3.6a}$$
$$\beta_{\mathbf{k}} = u_{\mathbf{k}}^{*} c_{-\mathbf{k}\downarrow} - v_{\mathbf{k}} c_{\mathbf{k}\uparrow}^{\dagger} \tag{3.6b}$$

the mean-field Hamiltonian is again of the form,

$$H_{MF} = \sum_{\mathbf{k}} \left[R_{\mathbf{k}} \alpha_{\mathbf{k}}^{\dagger} \alpha_{\mathbf{k}} - R_{\mathbf{k}} \beta_{\mathbf{k}} \beta_{\mathbf{k}}^{\dagger} + C_{\mathbf{k}} \alpha_{\mathbf{k}}^{\dagger} \beta_{\mathbf{k}}^{\dagger} + C_{\mathbf{k}}^{*} \beta_{\mathbf{k}} \alpha_{\mathbf{k}} \right] \tag{3.7}$$

where $R_{\mathbf{k}}$ and $C_{\mathbf{k}}$ are the same as in Eq. 1.6. The electromagnetic Hamiltonian terms are,

$$\begin{aligned} H_{EM}^{(1)} = \frac{e\hbar}{2m} \sum_{\mathbf{k},\mathbf{q}} (2\mathbf{k}+\mathbf{q}) \cdot \mathbf{A}_{\mathbf{q}}(\mathbf{t}) \Big[& (u_{\mathbf{k}+\mathbf{q}}^{*} u_{\mathbf{k}} + v_{\mathbf{k}+\mathbf{q}} v_{\mathbf{k}}^{*}) \alpha_{\mathbf{k}+\mathbf{q}}^{\dagger} \alpha_{\mathbf{k}} - (v_{\mathbf{k}+\mathbf{q}}^{*} v_{\mathbf{k}} + u_{\mathbf{k}}^{*} u_{\mathbf{k}+\mathbf{q}}) \beta_{\mathbf{k}}^{\dagger} \beta_{\mathbf{k}+\mathbf{q}} \\ & + (v_{\mathbf{k}+\mathbf{q}} u_{\mathbf{k}}^{*} - u_{\mathbf{k}+\mathbf{q}}^{*} v_{\mathbf{k}}) \alpha_{\mathbf{k}+\mathbf{q}}^{\dagger} \beta_{\mathbf{k}}^{\dagger} + (v_{\mathbf{k}}^{*} u_{\mathbf{k}+\mathbf{q}} - v_{\mathbf{k}+\mathbf{q}}^{*} u_{\mathbf{k}}) \beta_{\mathbf{k}+\mathbf{q}} \alpha_{\mathbf{k}} \Big] \end{aligned} \tag{3.8a}$$

$$\begin{aligned} H_{EM}^{(2)} = \frac{e^2}{2m} \sum_{\mathbf{k},\mathbf{q}} \left(\sum_{\mathbf{q}'} \mathbf{A}_{\mathbf{q}-\mathbf{q}'}(t) \cdot \mathbf{A}_{\mathbf{q}'}(t) \right) \Big[& (u_{\mathbf{k}+\mathbf{q}}^{*} u_{\mathbf{k}} - v_{\mathbf{k}+\mathbf{q}} v_{\mathbf{k}}^{*}) \alpha_{\mathbf{k}+\mathbf{q}}^{\dagger} \alpha_{\mathbf{k}} - (v_{\mathbf{k}+\mathbf{q}}^{*} v_{\mathbf{k}} - u_{\mathbf{k}}^{*} u_{\mathbf{k}+\mathbf{q}}) \beta_{\mathbf{k}}^{\dagger} \beta_{\mathbf{k}+\mathbf{q}} \\ & - (v_{\mathbf{k}+\mathbf{q}} u_{\mathbf{k}}^{*} + u_{\mathbf{k}+\mathbf{q}}^{*} v_{\mathbf{k}}) \alpha_{\mathbf{k}+\mathbf{q}}^{\dagger} \beta_{\mathbf{k}}^{\dagger} - (v_{\mathbf{k}}^{*} u_{\mathbf{k}+\mathbf{q}} + v_{\mathbf{k}+\mathbf{q}}^{*} u_{\mathbf{k}}) \beta_{\mathbf{k}+\mathbf{q}} \alpha_{\mathbf{k}} \Big] \end{aligned} \tag{3.8b}$$

The same shorthand is employed as before,

$$\begin{aligned} L_{\mathbf{k},\mathbf{q}}^{\pm} &= u_{\mathbf{k}+\mathbf{q}} u_{\mathbf{k}} \pm v_{\mathbf{k}+\mathbf{q}} v_{\mathbf{k}} \\ M_{\mathbf{k},\mathbf{q}}^{\pm} &= u_{\mathbf{k}+\mathbf{q}} v_{\mathbf{k}} \pm v_{\mathbf{k}+\mathbf{q}} u_{\mathbf{k}} \end{aligned} \tag{3.9}$$

3.3 Time-dependent ansatz

We need to develop a time-dependent operator ansatz, which will allow us to calculate the values of $\alpha^\dagger_{\mathbf{k}}(t)$, $\beta^\dagger_{\mathbf{k}}(t)$ – and thus also $c^\dagger_{\mathbf{k},\sigma}(t)$ and $c_{\mathbf{k},\sigma}(t)$ and all relevant two-time Green's functions. Our time-dependent ansatz is of the form [19–21],

$$\alpha^\dagger_{\mathbf{k}}(t) = \sum_\delta [a_{\mathbf{k}+\delta}(t)\alpha^\dagger_{\mathbf{k}+\delta} + b_{\mathbf{k}+\delta}(t)\beta_{\mathbf{k}+\delta} + ... \tag{3.10}$$

where we maintain our original time-independent operator basis, but take into account time-dependent prefactors and mixing with the other operators in our basis. This ansatz arises from the Heisenberg picture for the time-dependence of the Hamiltonian. In the Heisenberg picture, due to the time-dependence of the Hamiltonian, $H(t)$, a time-dependent operator, $U(t, t_0)$ is introduced given by,

$$U(t, t_0) = \exp\left(-i\int_{t_0}^{t} H(t')dt'\right) \tag{3.11}$$

which yields a simple expression for the time-dependence of $U(t, t_0)$,

$$i\hbar\frac{\partial}{\partial t}U(t, t_0) = H(t)U(t, t_0) \tag{3.12}$$

The time-dependence of a given operator can then be calculated from some initial value t_0, which can be set to zero for simplicity,

$$A(t) = U^\dagger(t)A(0)U(t) \tag{3.13}$$

This results in the very simple equation for the time evolution of $A(t)$,

$$\begin{aligned} i\hbar\frac{d}{dt}A(t) &= i\hbar\frac{d}{dt}U^\dagger(t)A(0)U(t) + i\hbar U^\dagger(t)A(0)\frac{d}{dt}U(t) && \text{(3.14a)}\\ &= -U^\dagger(t)H(t)A(0)U(t) + U^\dagger(t)A(0)H(t)U(t) && \text{(3.14b)}\\ &= [U^\dagger(t)A(0)U(t), U^\dagger(t)H(t)U(t)] && \text{(3.14c)}\\ &= [A(t), \tilde{H}(t)] && \text{(3.14d)} \end{aligned}$$

with $\tilde{H}(t)$ given by, $\tilde{H}(t) = U^\dagger(t)H(t)U(t)$. Under this transformation, it is possible to calculate the new Hamiltonian in terms of the time-dependent operators.

Our ansatz for the time-dependence of the operators arises from this equation in the following way. If we begin with the simple assumption that for the time-dependence of our operator $A(t) = a(t)A$, then by calculating the commutation relations, depending on the details of the Hamiltonian, we either can arrive at a closed form for the time-dependence of our prefactor $a(t)$, or introduce further time-dependent prefactors for another operator in the system. If the latter is the case, our first assumption is adjusted by adding the new operator and prefactor, and now take into account that the Hamiltonian, $\tilde{H}(t)$ has changed as well. This process can then be repeated to improve the accuracy of the time-dependence by adding in additional terms for more operators in the system. Alternatively, one can make a truncation by commuting the current ansatz for the time-dependence with the newly derived Hamiltonian.

3.3.1 Model Hamiltonian with the ansatz

Fortunately, our Hamiltonian is bilinear. Therefore, when we apply this method to our Hamiltonian, the time-dependent ansatz for our operators depends only on two of our time-independent operators,

$$\alpha^\dagger_{\mathbf{k}}(t) = \sum_\delta l_{\mathbf{k},\delta}(t)\alpha^\dagger_{\mathbf{k}+\delta} + m_{\mathbf{k},\delta}(t)\beta_{\mathbf{k}+\delta} \tag{3.15a}$$

$$\beta^\dagger_{\mathbf{k}}(t) = \sum_\delta n_{\mathbf{k},\delta}(t)\beta^\dagger_{\mathbf{k}+\delta} + o_{\mathbf{k},\delta}(t)\alpha_{\mathbf{k}+\delta} \tag{3.15b}$$

with the initial conditions that $l_{\mathbf{k}}(0) = 1$, $n_{\mathbf{k}}(0) = 1$, $l_{\mathbf{k},\delta} = n_{\mathbf{k},\delta} = 0\ \forall\ \delta$ s.t. $\delta \neq 0$ and $m_{\mathbf{k},\delta}(0) = o_{\mathbf{k},\delta}(0) = 0\ \forall\ \delta$. δ can, in general, correspond to some arbitrary momentum transfer from the commutator with the electromagnetic part of the Hamiltonian. However, in the next section, we limit the pump to a single momentum, which will restrict δ to integer multiples of the momentum $\mathbf{q}$ corresponding to to the chosen value for the pumping pulse $\mathbf{A}_\mathbf{q}$.

Though in the previous chapter it was beneficial to break up the electromagnetic Hamiltonian into linear and quadratic parts to differentiate between the quadratic excitations generated by the pump and the linear response of the probe, we will now focus solely on the former and so work with a single electromagnetic term. Our Hamiltonian in terms of our ansatz is now,

$$\tilde{H} = \tilde{H}_{MF} + \tilde{H}_{EM} \tag{3.16}$$

with $\tilde{H}_{MF}$ given now in terms of the new ansatz for our operators as

$$\begin{aligned}
\tilde{H}_{MF} = \sum_{\mathbf{k},\delta,\eta} \Big[& \alpha^\dagger_{\mathbf{k}+\delta}\alpha_{\mathbf{k}+\eta}\Big((l_{\mathbf{k},\delta}l^*_{\mathbf{k},\eta} - o^*_{\mathbf{k},\delta}o_{\mathbf{k},\eta})R_\mathbf{k} + (l_{\mathbf{k},\delta}o_{\mathbf{k},\eta})C_\mathbf{k} + (l^*_{\mathbf{k},\eta}o^*_{\mathbf{k},\delta})C^*_\mathbf{k}\Big) \\
& + \beta^\dagger_{\mathbf{k}+\eta}\beta_{\mathbf{k}+\delta}\Big((-m^*_{\mathbf{k},\eta}m_{\mathbf{k},\delta} + n_{\mathbf{k},\eta}n^*_{\mathbf{k},\delta})R_\mathbf{k} + (-m_{\mathbf{k},\delta}n_{\mathbf{k},\eta})C_\mathbf{k} - (m^*_{\mathbf{k},\eta}n^*_{\mathbf{k},\delta})C^*_\mathbf{k}\Big) \\
& + \alpha^\dagger_{\mathbf{k}+\delta}\beta^\dagger_{\mathbf{k}+\eta}\Big((l_{\mathbf{k},\delta}m^*_{\mathbf{k},\eta} - n_{\mathbf{k},\eta}o^*_{\mathbf{k},\delta})R_\mathbf{k} + (l_{\mathbf{k},\delta}n_{\mathbf{k},\eta})C_\mathbf{k} + (o^*_{\mathbf{k},\delta}m^*_{\mathbf{k},\eta})C^*_\mathbf{k}\Big) \\
& + \beta_{\mathbf{k}+\delta}\alpha_{\mathbf{k}+\eta}\Big((m_{\mathbf{k},\delta}l^*_{\mathbf{k},\eta} - n^*_{\mathbf{k},\delta}o_{\mathbf{k},\eta})R_\mathbf{k} + (m_{\mathbf{k},\delta}o_{\mathbf{k},\eta})C_\mathbf{k} + (n^*_{\mathbf{k},\delta}l^*_{\mathbf{k},\eta})C^*_\mathbf{k}\Big) \\
& + \delta_{\delta,\eta}\Big((-o^*_{\mathbf{k},\delta}o_{\mathbf{k},\eta} + m^*_{\mathbf{k},\eta}m_{\mathbf{k},\delta})R_\mathbf{k} + (m_{\mathbf{k},\delta}n_{\mathbf{k},\eta})C_\mathbf{k} + (m^*_{\mathbf{k},\eta}n^*_{\mathbf{k},\delta})C^*_\mathbf{k}\Big)\Big].
\end{aligned} \tag{3.17}$$

The explicit time-dependence of l, m, n and o has been excluded for compactness. We can simplify the Hamiltonian slightly by dropping the last term in the Hamiltonian, as it only amounts to a constant energy offset and does not effect the dynamics of the system. $\tilde{H}_{EM}$ given in terms of the new ansatz for our operators is,

$$
\begin{aligned}
\tilde{H}_{EM} = & \\
&\Big[\frac{e\hbar}{2m}\sum_{\mathbf{k},\mathbf{q},\delta,\eta}(2\mathbf{k}+\mathbf{q})A_{\mathbf{q}}\Big]\times \\
&\Big[\alpha^{\dagger}_{\mathbf{k}+\mathbf{q}+\delta}\alpha_{\mathbf{k}+\eta}\Big((l_{\mathbf{k}+\mathbf{q},\delta}l^{*}_{\mathbf{k},\eta}+o^{*}_{\mathbf{k}+\mathbf{q},\delta}o_{\mathbf{k},\eta})L^{+}_{\mathbf{k},\mathbf{q}}+(-l_{\mathbf{k}+\mathbf{q},\delta}o_{\mathbf{k},\eta}+o^{*}_{\mathbf{k}+\mathbf{q},\delta}l^{*}_{\mathbf{k},\eta})M^{-}_{\mathbf{k},\mathbf{q}}\Big) \\
&+\beta^{\dagger}_{\mathbf{k}+\eta}\beta_{\mathbf{k}+\mathbf{q}+\delta}\Big((-m^{*}_{\mathbf{k},\eta}m_{\mathbf{k}+\mathbf{q},\delta}-n_{\mathbf{k},\eta}n^{*}_{\mathbf{k}+\mathbf{q},\delta})L^{+}_{\mathbf{k},\mathbf{q}}+(+m_{\mathbf{k}+\mathbf{q},\delta}n_{\mathbf{k},\eta}-n^{*}_{\mathbf{k}+\mathbf{q},\delta}m^{*}_{\mathbf{k},\eta})M^{-}_{\mathbf{k},\mathbf{q}}\Big) \\
&+\alpha^{\dagger}_{\mathbf{k}+\mathbf{q}+\delta}\beta^{\dagger}_{\mathbf{k}+\eta}\Big((l_{\mathbf{k}+\mathbf{q},\delta}m^{*}_{\mathbf{k},\eta}+n_{\mathbf{k},\eta}o^{*}_{\mathbf{k}+\mathbf{q},\delta})L^{+}_{\mathbf{k},\mathbf{q}}+(-l_{\mathbf{k}+\mathbf{q},\delta}n_{\mathbf{k},\eta}+o^{*}_{\mathbf{k}+\mathbf{q},\delta}m^{*}_{\mathbf{k},\eta})M^{-}_{\mathbf{k},\mathbf{q}}\Big) \\
&+\beta_{\mathbf{k}+\mathbf{q}+\delta}\alpha_{\mathbf{k}+\eta}\Big((m_{\mathbf{k}+\mathbf{q},\delta}l^{*}_{\mathbf{k},\eta}+n^{*}_{\mathbf{k}+\mathbf{q},\delta}o_{\mathbf{k},\eta})L^{+}_{\mathbf{k},\mathbf{q}}+(-m_{\mathbf{k}+\mathbf{q},\delta}o_{\mathbf{k},\eta}+n^{*}_{\mathbf{k}+\mathbf{q},\delta}l^{*}_{\mathbf{k},\eta})M^{-}_{\mathbf{k}}\Big) \\
&+\delta_{\delta+q,\eta}\Big((-o^{*}_{\mathbf{k}+\mathbf{q},\delta}o_{\mathbf{k},\eta}+m^{*}_{\mathbf{k},\eta}m_{\mathbf{k}+\mathbf{q},\delta})L^{+}_{\mathbf{k},\mathbf{q}}+(m_{\mathbf{k}+\mathbf{q},\delta}n_{\mathbf{k},\eta}+n^{*}_{\mathbf{k}+\mathbf{q},\delta}m^{*}_{\mathbf{k},\eta})M^{-}_{\mathbf{k},\mathbf{q}}\Big)\Big] \\
&+\frac{e^{2}}{2m}\sum_{\mathbf{k},\mathbf{q},\delta,\eta}\Big(\sum_{\mathbf{q}'}A_{\mathbf{q}-\mathbf{q}'}\cdot A_{\mathbf{q}'}\Big) \\
&\Big[\alpha^{\dagger}_{\mathbf{k}+\mathbf{q}+\delta}\alpha_{\mathbf{k}+\eta}\Big((l_{\mathbf{k}+\mathbf{q},\delta}l^{*}_{\mathbf{k},\eta}-o^{*}_{\mathbf{k}+\mathbf{q},\delta}o_{\mathbf{k},\eta})L^{-}_{\mathbf{k},\mathbf{q}}-(l_{\mathbf{k}+\mathbf{q},\delta}o_{\mathbf{k},\eta}+o^{*}_{\mathbf{k}+\mathbf{q},\delta}l^{*}_{\mathbf{k},\eta})M^{+}_{\mathbf{k},\mathbf{q}}\Big) \\
&+\beta^{\dagger}_{\mathbf{k}+\eta}\beta_{\mathbf{k}+\mathbf{q}+\delta}\Big((-m^{*}_{\mathbf{k},\eta}m_{\mathbf{k}+\mathbf{q},\delta}+n_{\mathbf{k},\eta}n^{*}_{\mathbf{k}+\mathbf{q},\delta})L^{-}_{\mathbf{k},\mathbf{q}}-(-m_{\mathbf{k}+\mathbf{q},\delta}n_{\mathbf{k},\eta}-n^{*}_{\mathbf{k}+\mathbf{q},\delta}m^{*}_{\mathbf{k},\eta})M^{+}_{\mathbf{k},\mathbf{q}}\Big) \\
&+\alpha^{\dagger}_{\mathbf{k}+\mathbf{q}+\delta}\beta^{\dagger}_{\mathbf{k}+\eta}\Big((l_{\mathbf{k}+\mathbf{q},\delta}m^{*}_{\mathbf{k},\eta}-n_{\mathbf{k},\eta}o^{*}_{\mathbf{k}+\mathbf{q},\delta})L^{-}_{\mathbf{k},\mathbf{q}}-(l_{\mathbf{k}+\mathbf{q},\delta}n_{\mathbf{k},\eta}+o^{*}_{\mathbf{k}+\mathbf{q},\delta}m^{*}_{\mathbf{k},\eta})M^{+}_{\mathbf{k},\mathbf{q}}\Big) \\
&+\beta_{\mathbf{k}+\mathbf{q}+\delta}\alpha_{\mathbf{k}+\eta}\Big((m_{\mathbf{k}+\mathbf{q},\delta}l^{*}_{\mathbf{k},\eta}-n^{*}_{\mathbf{k}+\mathbf{q},\delta}o_{\mathbf{k},\eta})L^{-}_{\mathbf{k},\mathbf{q}}-(m_{\mathbf{k}+\mathbf{q},\delta}o_{\mathbf{k},\eta}+n^{*}_{\mathbf{k}+\mathbf{q},\delta}l^{*}_{\mathbf{k},\eta})M^{+}_{\mathbf{k}}\Big) \\
&+\delta_{\delta+q,\eta}\Big((-o^{*}_{\mathbf{k}+\mathbf{q},\delta}o_{\mathbf{k},\eta}+m^{*}_{\mathbf{k},\eta}m_{\mathbf{k}+\mathbf{q},\delta})L^{+}_{\mathbf{k},\mathbf{q}}+(m_{\mathbf{k}+\mathbf{q},\delta}n_{\mathbf{k},\eta}+n^{*}_{\mathbf{k}+\mathbf{q},\delta}m^{*}_{\mathbf{k},\eta})M^{-}_{\mathbf{k},\mathbf{q}}\Big)\Big]
\end{aligned}
\tag{3.18}
$$

Again, we can drop the last term as it only amounts to a constant offset in our Hamiltonian.

We can also write an expression for the order parameter $\Delta_{\mathbf{k}}(t)$ in terms of the ansatz for our new operators. Beginning with a modified Eq. 2.10 for the now explicit time-dependence of our operators,

$$
\Delta_{\mathbf{k}'}(t)=\frac{1}{N}\sum_{\mathbf{k}\in\mathcal{W}}V_{\mathbf{k},\mathbf{k}'}\Big(u_{\mathbf{k}}v_{\mathbf{k}}(1-\langle\alpha^{\dagger}_{\mathbf{k}}(t)\alpha_{\mathbf{k}}(t)\rangle-\langle\beta^{\dagger}_{\mathbf{k}}(t)\beta_{\mathbf{k}}(t)\rangle)+u^{2}_{\mathbf{k}}\langle\beta_{\mathbf{k}}(t)\alpha_{\mathbf{k}}(t)\rangle-v^{2}_{\mathbf{k}}\langle\alpha^{\dagger}_{\mathbf{k}}(t)\beta^{\dagger}_{\mathbf{k}}(t)\Big). \tag{3.19}
$$

We must calculate the expectation values for our new operators in terms of our ansatz. The first expectation value is given by,

$$
\langle\alpha^{\dagger}_{\mathbf{k}}(t)\alpha_{\mathbf{k}}(t)\rangle=\langle\Big(\sum_{\rho}l_{\mathbf{k},\rho}(t)\alpha^{\dagger}_{\mathbf{k}+\rho}+m_{\mathbf{k},\rho}(t)\beta_{\mathbf{k}+\rho}\Big)\Big(\sum_{\delta}l^{*}_{\mathbf{k},\rho}(t)\alpha_{\mathbf{k}+\rho}+m^{*}_{\mathbf{k},\rho}(t)\beta^{\dagger}_{\mathbf{k}+\rho}\Big)\rangle \tag{3.20}
$$

and due to the fact that, for general operators A and B, $\langle A^{\dagger}B\rangle=0$ and $\langle AB^{\dagger}\rangle=\delta_{A,B}$ we get a

simple expression for $\langle \alpha^\dagger_{\mathbf{k}}(t)\alpha_{\mathbf{k}}(t)\rangle$ and the three subsequent expectation values,

$$\langle \alpha^\dagger_{\mathbf{k}}\alpha_{\mathbf{k}}\rangle = \sum_\rho |m_{\mathbf{k},\rho}(t)|^2 \tag{3.21a}$$

$$\langle \beta^\dagger_{\mathbf{k}}\beta_{\mathbf{k}}\rangle = \sum_\rho |o_{\mathbf{k},\rho}(t)|^2 \tag{3.21b}$$

$$\langle \beta_{\mathbf{k}}\alpha_{\mathbf{k}}\rangle = \sum_\rho n^*_{\mathbf{k},\rho}(t)m^*_{\mathbf{k},\rho}(t) \tag{3.21c}$$

$$\langle \alpha^\dagger_{\mathbf{k}}\beta^\dagger_{\mathbf{k}}\rangle = \sum_\rho n_{\mathbf{k},\rho}(t)m_{\mathbf{k},\rho}(t) \tag{3.21d}$$

Clearly the final two expectation values are the complex conjugate of each other, since l, m, n and o are simple complex numbers. Therefore, we can rewrite our equation for the gap parameter $\Delta_{\mathbf{k}'}(t)$ as,

$$\Delta_{\mathbf{k}'}(t) = \frac{1}{N}\sum_{\mathbf{k}\in\mathcal{W},\rho} V_{\mathbf{k},\mathbf{k}'}\Big(u_{\mathbf{k}}v_{\mathbf{k}}(1-|m_{\mathbf{k},\rho}(t)|^2-|o_{\mathbf{k},\rho}(t)|^2)+u^2_{\mathbf{k}}n^*_{\mathbf{k},\rho}(t)m^*_{\mathbf{k},\rho}(t)-v^2_{\mathbf{k}}n_{\mathbf{k},\rho}(t)m_{\mathbf{k},\rho}(t)\Big) \tag{3.22}$$

It is a simple matter to also calculate the other four expectation values for the remaining two operator combinations, which will be useful for calculating the Green's functions later:

$$\langle \alpha_{\mathbf{k}}(t)\alpha^\dagger_{\mathbf{k}}(t)\rangle = \sum_\rho |l_{\mathbf{k},\rho}(t)|^2 \tag{3.23a}$$

$$\langle \beta_{\mathbf{k}}(t)\beta^\dagger_{\mathbf{k}}(t)\rangle = \sum_\rho |n_{\mathbf{k},\rho}(t)|^2 \tag{3.23b}$$

$$\langle \alpha_{\mathbf{k}}(t)\beta_{\mathbf{k}}(t)\rangle = \sum_\rho l^*_{\mathbf{k},\rho}(t)o^*_{\mathbf{k},\rho}(t) \tag{3.23c}$$

$$\langle \beta^\dagger_{\mathbf{k}}(t)\alpha^\dagger_{\mathbf{k}}(t)\rangle = \sum_\rho l_{\mathbf{k},\rho}(t)o_{\mathbf{k},\rho}(t) \tag{3.23d}$$

3.4 Equations of Motion

We now derive the new equations of motion in terms of the time-dependent operators. In fact, the time-dependent equations of motion are now equations of motion for the prefactors in our ansatz. Following the same methodology as in the previous chapter, we work with the Heisenberg equations of motion. Our operators have an explicit time-dependent term now, however we assume that the change in our operators is small compared to the commutator term. This should be justified given that we imposed the time-dependence as part of our ansatz; had we not, the operators would have no explicit time-dependence. This should be equivalent to the time-independent basis of the previous chapter, since in both cases no time-dependence will be incurred beyond terms coming from the

commutator with the Hamiltonian. The equations of motion are:

$$i\hbar\frac{d}{dt}\alpha^\dagger_{\mathbf{k}}(t) = \left[\alpha^\dagger_{\mathbf{k}}(t), \tilde{H}\right] \tag{3.24a}$$

$$i\hbar\sum_\rho\left(\frac{d}{dt}l_{\mathbf{k},\rho}(t)\alpha^\dagger_{\mathbf{k}+\rho} + \frac{d}{dt}m_{\mathbf{k},\rho}(t)\beta_{\mathbf{k}+\rho}\right) = \left[\alpha^\dagger_{\mathbf{k}}(t), \tilde{H}_{sc} + \tilde{H}_{em}\right], \tag{3.24b}$$

$$i\hbar\frac{d}{dt}\beta^\dagger_{\mathbf{k}}(t) = \left[\beta^\dagger_{\mathbf{k}}(t), \tilde{H}\right] \tag{3.25a}$$

$$i\hbar\sum_\rho\left(\frac{d}{dt}n_{\mathbf{k},\rho}(t)\beta^\dagger_{\mathbf{k}+\rho} + \frac{d}{dt}o_{\mathbf{k},\rho}(t)\alpha_{\mathbf{k}+\rho}\right) = \left[\beta^\dagger_{\mathbf{k}}(t), \tilde{H}_{sc} + \tilde{H}_{em}\right]. \tag{3.25b}$$

ρ will be some integer multiple of the transferred momentum $\mathbf{q}$ from the electromagnetic portion of the Hamiltonian. For a relatively small total incident energy, the additional terms in ρ are proportionally small to the power of the integer, so sum will converge on short time-scales beyond some sufficiently large cutoff integer.

As before, we define the vector potential for the pump $\mathbf{A}_{\mathbf{q}}(t)$,

$$\mathbf{A}_{\mathbf{q}}(t) = \mathbf{A}_{\mathrm{p}}\ \exp\left[-\left(\frac{2\sqrt{\ln 2}t}{\tau}\right)^2\right](\delta_{\mathbf{q},\mathbf{q}_0}e^{-i\omega_p t} + \delta_{\mathbf{q},-\mathbf{q}_0}e^{i\omega_p t}) \tag{3.26}$$

where the amplitude of the pump is $\mathbf{A}_p$ and the full width at half maximum is τ_p. The pumping frequency and momentum are given by ω_p and $\mathbf{q_p}$. We choose a linear polarization for $\mathbf{A_p}$ such that the momentum vector $\mathbf{q}_p$ and the vector potential $\mathbf{A_q}(t)$ are perpendicular vectors as required by electromagnetic theory. Since we have once again chosen the form of a monochromatic pump (and vector potential), the equations of motion will only couple terms of integer multiples of the transferred momentum $\mathbf{q}$.

While we now only have two explicit equations to solve, our operators (and our Hamiltonian) are significantly more complicated. The $\alpha^\dagger_{\mathbf{k}}$ commutator with the electromagnetic part of the Hamiltonian is as follows,

$$
\begin{aligned}
&\left[\alpha^{\dagger}_{\mathbf{k}'}(t), \tilde{H}_{em}\right] \\
&\quad = \left[\frac{e\hbar}{2m}\sum_{\mathbf{k},\mathbf{q},\delta,\eta,\gamma}(2\mathbf{k}+\mathbf{q})A_{\mathbf{q}}\right]\times \\
&\Bigg[\alpha^{\dagger}_{\mathbf{k}+\mathbf{q}+\delta}(-\delta_{\mathbf{k}'+\gamma,\mathbf{k}+\eta})\Big(l_{\mathbf{k}',\gamma}\Big((l_{\mathbf{k}+\mathbf{q},\delta}l^{*}_{\mathbf{k},\eta}+o^{*}_{\mathbf{k}+\mathbf{q},\delta}o_{\mathbf{k},\eta})L^{+}_{\mathbf{k},\mathbf{q}}+(-l_{\mathbf{k}+\mathbf{q},\delta}o_{\mathbf{k},\eta}+o^{*}_{\mathbf{k}+\mathbf{q},\delta}l^{*}_{\mathbf{k},\eta})M^{-}_{\mathbf{k},\mathbf{q}}\Big) \\
&\qquad\qquad + m_{\mathbf{k}',\gamma}\Big((l_{\mathbf{k}+\mathbf{q},\delta}m^{*}_{\mathbf{k},\eta}+n_{\mathbf{k},\eta}o^{*}_{\mathbf{k}+\mathbf{q},\delta})L^{+}_{\mathbf{k},\mathbf{q}}+(-l_{\mathbf{k}+\mathbf{q},\delta}n_{\mathbf{k},\eta}+o^{*}_{\mathbf{k}+\mathbf{q},\delta}m^{*}_{\mathbf{k},\eta})M^{-}_{\mathbf{k},\mathbf{q}}\Big)\Big) \\
&+\beta_{\mathbf{k}+\mathbf{q}+\delta}(\delta_{\mathbf{k}'+\gamma,\mathbf{k}+\eta})\quad \Big(m_{\mathbf{k}',\gamma}\Big((-m^{*}_{\mathbf{k},\eta}m_{\mathbf{k}+\mathbf{q},\delta}-n_{\mathbf{k},\eta}n^{*}_{\mathbf{k}+\mathbf{q},\delta})L^{+}_{\mathbf{k},\mathbf{q}}+(+m_{\mathbf{k}+\mathbf{q},\delta}n_{\mathbf{k},\eta}-n^{*}_{\mathbf{k}+\mathbf{q},\delta}m^{*}_{\mathbf{k},\eta})M^{-}_{\mathbf{k},\mathbf{q}}\Big) \\
&\qquad\qquad - l_{\mathbf{k}',\gamma}\Big((m_{\mathbf{k}+\mathbf{q},\delta}l^{*}_{\mathbf{k},\eta}+n^{*}_{\mathbf{k}+\mathbf{q},\delta}o_{\mathbf{k},\eta})L^{+}_{\mathbf{k},\mathbf{q}}+(-m_{\mathbf{k}+\mathbf{q},\delta}o_{\mathbf{k},\eta}+n^{*}_{\mathbf{k}+\mathbf{q},\delta}l^{*}_{\mathbf{k},\eta})M^{-}_{\mathbf{k},\mathbf{q}}\Big)\Big)\Bigg] \\
&\quad + \left[\frac{e^2}{2m}\sum_{\mathbf{k},\mathbf{q},\delta,\eta,\gamma}\Big(\sum_{\mathbf{q}'}A_{\mathbf{q}-\mathbf{q}'}\cdot A_{\mathbf{q}'}\Big)\right]\times \\
&\Bigg[\alpha^{\dagger}_{\mathbf{k}+\mathbf{q}+\delta}(-\delta_{\mathbf{k}'+\gamma,\mathbf{k}+\eta})\Big(l_{\mathbf{k}',\gamma}\Big((l_{\mathbf{k}+\mathbf{q},\delta}l^{*}_{\mathbf{k},\eta}-o^{*}_{\mathbf{k}+\mathbf{q},\delta}o_{\mathbf{k},\eta})L^{-}_{\mathbf{k},\mathbf{q}}-(l_{\mathbf{k}+\mathbf{q},\delta}o_{\mathbf{k},\eta}+o^{*}_{\mathbf{k}+\mathbf{q},\delta}l^{*}_{\mathbf{k},\eta})M^{+}_{\mathbf{k},\mathbf{q}}\Big) \\
&\qquad\qquad + m_{\mathbf{k}',\gamma}\Big((l_{\mathbf{k}+\mathbf{q},\delta}m^{*}_{\mathbf{k},\eta}-n_{\mathbf{k},\eta}o^{*}_{\mathbf{k}+\mathbf{q},\delta})L^{-}_{\mathbf{k},\mathbf{q}}-(l_{\mathbf{k}+\mathbf{q},\delta}n_{\mathbf{k},\eta}+o^{*}_{\mathbf{k}+\mathbf{q},\delta}m^{*}_{\mathbf{k},\eta})M^{+}_{\mathbf{k},\mathbf{q}}\Big)\Big) \\
&+\beta_{\mathbf{k}+\mathbf{q}+\delta}(\delta_{\mathbf{k}'+\gamma,\mathbf{k}+\eta})\quad \Big(m_{\mathbf{k}',\gamma}\Big((-m^{*}_{\mathbf{k},\eta}m_{\mathbf{k}+\mathbf{q},\delta}+n_{\mathbf{k},\eta}n^{*}_{\mathbf{k}+\mathbf{q},\delta})L^{-}_{\mathbf{k},\mathbf{q}}-(-m_{\mathbf{k}+\mathbf{q},\delta}n_{\mathbf{k},\eta}-n^{*}_{\mathbf{k}+\mathbf{q},\delta}m^{*}_{\mathbf{k},\eta})M^{+}_{\mathbf{k},\mathbf{q}}\Big) \\
&\qquad\qquad - l_{\mathbf{k}',\gamma}\Big((m_{\mathbf{k}+\mathbf{q},\delta}l^{*}_{\mathbf{k},\eta}-n^{*}_{\mathbf{k}+\mathbf{q},\delta}o_{\mathbf{k},\eta})L^{-}_{\mathbf{k},\mathbf{q}}-(m_{\mathbf{k}+\mathbf{q},\delta}o_{\mathbf{k},\eta}+n^{*}_{\mathbf{k}+\mathbf{q},\delta}l^{*}_{\mathbf{k},\eta})M^{+}_{\mathbf{k},\mathbf{q}}\Big)\Big)\Bigg]
\end{aligned}
\tag{3.27}
$$

and for $\beta^{\dagger}_{\mathbf{k}}$ we obtain a similar expression. Collecting like terms, we then get the following differential equations for the pre-factors of $\alpha^{\dagger}_{\mathbf{k}'}(t)$ by choosing $\mathbf{k}'+\rho=\mathbf{k}+\delta$ and $\mathbf{k}'+\rho=\mathbf{k}+\mathbf{q}+\delta$ in the subsequent 2 sums:

$$
\begin{aligned}
&i\hbar\frac{d}{dt}l_{\mathbf{k}',\rho}(t)\alpha^{\dagger}_{\mathbf{k}'+\rho} = \\
&-\sum_{\delta,\gamma}\alpha^{\dagger}_{\mathbf{k}'+\rho}\Big(l_{\mathbf{k}',\gamma}\Big((l_{\mathbf{k}'+\rho-\delta,\delta}l^{*}_{\mathbf{k}'+\rho-\delta,\gamma+\delta-\rho} - o^{*}_{\mathbf{k}'+\rho-\delta,\delta}o_{\mathbf{k}'+\rho-\delta,\gamma+\delta-\rho})R_{\mathbf{k}'+\rho-\delta} \\
&\qquad + (l_{\mathbf{k}'+\rho-\delta,\delta}o_{\mathbf{k}'+\rho-\delta,\gamma+\delta-\rho})C_{\mathbf{k}'+\rho-\delta} + (l^{*}_{\mathbf{k}'+\rho-\delta,\gamma+\delta-\rho}o^{*}_{\mathbf{k}'+\rho-\delta,\delta})C^{*}_{\mathbf{k}'+\rho-\delta}\Big) \\
&\quad + m_{\mathbf{k}',\gamma}\Big((l_{\mathbf{k}'+\rho-\delta,\delta}m^{*}_{\mathbf{k}'+\rho-\delta,\gamma+\delta-\rho} - n_{\mathbf{k}'+\rho-\delta,\gamma+\delta-\rho}o^{*}_{\mathbf{k}'+\rho-\delta,\delta})R_{\mathbf{k}'+\rho-\delta} \\
&\qquad + (l_{\mathbf{k}'+\rho-\delta,\delta}n_{\mathbf{k}'+\rho-\delta,\gamma+\delta-\rho})C_{\mathbf{k}'+\rho-\delta} + (o^{*}_{\mathbf{k}'+\rho-\delta,\delta}m^{*}_{\mathbf{k}'+\rho-\delta,\gamma+\delta-\rho})C^{*}_{\mathbf{k}'+\rho-\delta}\Big)\Big) \\
&-\Big[\frac{e\hbar}{2m}\sum_{\mathbf{q},\delta,\gamma}(2(\mathbf{k}'-\mathbf{q}+\rho-\delta)+\mathbf{q})A_{\mathbf{q}}\Big]\times \\
&\quad \alpha^{\dagger}_{\mathbf{k}'+\rho}\Big(l_{\mathbf{k}',\gamma}\Big((l_{\mathbf{k}'+\rho-\delta,\delta}l^{*}_{\mathbf{k}'+\rho-\delta-q,\gamma+\delta+q-\rho} + o^{*}_{\mathbf{k}'+\rho-\delta,\delta}o_{\mathbf{k}'+\rho-\delta-q,\gamma+\delta+q-\rho})L^{+}_{\mathbf{k}'-\mathbf{q}+\rho-\delta,\mathbf{q}} \\
&\qquad + (-l_{\mathbf{k}'+\rho-\delta,\delta}o_{\mathbf{k}'+\rho-\delta-q,\gamma+\delta+q-\rho} + o^{*}_{\mathbf{k}'+\rho-\delta,\delta}l^{*}_{\mathbf{k}'+\rho-\delta-q,\gamma+\delta+q-\rho})M^{-}_{\mathbf{k}'-\mathbf{q}+\rho-\delta,\mathbf{q}}\Big) \\
&\quad + m_{\mathbf{k}',\gamma}\Big((l_{\mathbf{k}'+\rho-\delta,\delta}m^{*}_{\mathbf{k}'+\rho-\delta-q,\gamma+\delta+q-\rho} + n_{\mathbf{k}'+\rho-\delta-q,\gamma+\delta+q-\rho}o^{*}_{\mathbf{k}'+\rho-\delta,\delta})L^{+}_{\mathbf{k}'-\mathbf{q}+\rho-\delta,\mathbf{q}} \\
&\qquad + (-l_{\mathbf{k}'+\rho-\delta,\delta}n_{\mathbf{k}'+\rho-\delta-q,\gamma+\delta+q-\rho} + o^{*}_{\mathbf{k}'+\rho-\delta,\delta}m^{*}_{\mathbf{k}'+\rho-\delta-q,\gamma+\delta+q-\rho})M^{-}_{\mathbf{k}'-\mathbf{q}+\rho-\delta,\mathbf{q}}\Big)\Big) \\
&-\Big[\frac{e^2}{2m}\sum_{\mathbf{q},\delta,\gamma}\Big(\sum_{\mathbf{q}'}A_{\mathbf{q}-\mathbf{q}'}\cdot A_{\mathbf{q}'}\Big)\Big]\times \\
&\quad \alpha^{\dagger}_{\mathbf{k}'+\rho}\Big(l_{\mathbf{k}',\gamma}\Big((l_{\mathbf{k}'+\rho-\delta,\delta}l^{*}_{\mathbf{k}'+\rho-\delta-q,\gamma+\delta+q-\rho} - o^{*}_{\mathbf{k}'+\rho-\delta,\delta}o_{\mathbf{k}'+\rho-\delta-q,\gamma+\delta+q-\rho})L^{-}_{\mathbf{k}'-\mathbf{q}+\rho-\delta,\mathbf{q}} \\
&\qquad - (l_{\mathbf{k}'+\rho-\delta,\delta}o_{\mathbf{k}'+\rho-\delta-q,\gamma+\delta+q-\rho} + o^{*}_{\mathbf{k}'+\rho-\delta,\delta}l^{*}_{\mathbf{k}'+\rho-\delta-q,\gamma+\delta+q-\rho})M^{+}_{\mathbf{k}'-\mathbf{q}+\rho-\delta,\mathbf{q}}\Big) \\
&\quad + m_{\mathbf{k}',\gamma}\Big((l_{\mathbf{k}'+\rho-\delta,\delta}m^{*}_{\mathbf{k}'+\rho-\delta-q,\gamma+\delta+q-\rho} - n_{\mathbf{k}'+\rho-\delta-q,\gamma+\delta+q-\rho}o^{*}_{\mathbf{k}'+\rho-\delta,\delta})L^{-}_{\mathbf{k}'-\mathbf{q}+\rho-\delta,\mathbf{q}} \\
&\qquad - (l_{\mathbf{k}'+\rho-\delta,\delta}n_{\mathbf{k}'+\rho-\delta-q,\gamma+\delta+q-\rho} + o^{*}_{\mathbf{k}'+\rho-\delta,\delta}m^{*}_{\mathbf{k}'+\rho-\delta-q,\gamma+\delta+q-\rho})M^{+}_{\mathbf{k}'-\mathbf{q}+\rho-\delta,\mathbf{q}}\Big)\Big)
\end{aligned}
\tag{3.28}
$$

and again similar expressions are found for the $\beta_{\mathbf{k}}$, $\alpha_{\mathbf{k}}$ and $\beta^{\dagger}_{\mathbf{k}}$ operators.

3.4.1 Initial conditions and numerical approximations

In order to limit the number of equations in our system, one must choose an upper bound N such that, $|\gamma|, |\delta|, |\rho|, \eta \leq N\mathbf{q}\ \forall\ \frac{\eta}{\mathbf{q}},\ \frac{\gamma}{\mathbf{q}}, \frac{\delta}{\mathbf{q}}, \frac{\rho}{\mathbf{q}}, N \in \mathcal{Z}$. We will set the coefficients outside of this bound to zero. In practice, N is chosen so that the equations are sufficiently convergent within the time domain of interest. Convergence will, in general, not be expected for all forms of an electromagnetic term, however, we will enforce a pump with a sufficiently small amplitude that convergence can be reached for a reasonable number of terms. This is because nonzero integer terms will scale as powers of $\mathbf{A}^{z}_{0}$. With this choice of N, our sum now becomes limited in the following way:

1) Since we have chosen $\mathbf{k}'+\gamma = \mathbf{k}+\eta$ and $\mathbf{k}'+\rho = \mathbf{k}+\delta$ in the first sum of Eq. 3.28 and A.4, we have the following additional restriction that, given $\rho, \delta,\ \gamma \in [-N\mathbf{q}, N\mathbf{q}]$ *s.t.* $|\rho-\delta-\gamma| \leq N\mathbf{q}$.

2) In the subsequent sums of Eq. 3.28 and A.4, we choose $\mathbf{k}'+\gamma = \mathbf{k}+\eta$ and $\mathbf{k}'+\rho = \mathbf{k}+\mathbf{q}+\delta$ so

Parameters			
Superconductor		Pump	
a	10^{-10} m	$\hbar\omega_{\rm p}$	6.0 meV
E_F	9470 meV	$\omega_{\rm p}$	9.12×10^{-3} fs^{-1}
m	$1.9m_e$	$A_{\rm p}$	$1.0\times10^{-8}\frac{\rm J\ s}{\rm C\ m}$
w_c	8.3 meV	$\tau_{\rm p}$	100 fs^{-1}
Δ_0	1.35 meV	$q_{\rm p}\ a$	3.04×10^{-6}

Table 3.1: Parameters for our calculations. a is the lattice spacing, E_F is the Fermi energy, m is the re-normalized mass and w_c is the cutoff frequency. Δ_0 is the initial size of the gap before the pump is turned on. $\omega_{p/pr}$, $A_{p/pr}$, $\tau_{p/pr}$ and $q_{p/pr}$ are the pump/probe frequency, amplitude, full width at half maximum and momentum.

that we get the additional restriction that, given $\rho,\delta,\ \gamma\in[-N\mathbf{q},N\mathbf{q}]\ s.t.\ |\rho-\delta-\mathbf{q}-\gamma|\leq N\mathbf{q}$

3) Since we have chosen $\mathbf{k}'+\gamma=\mathbf{k}+\delta$ and $\mathbf{k}'+\rho=\mathbf{k}+\eta$ in the first sum of Eq. A.5 and A.6, we have the following additional restriction that, given $\rho,\eta,\ \gamma\in[-N\mathbf{q},N\mathbf{q}]\ s.t.\ |\rho-\eta-\gamma|\leq N\mathbf{q}$.

4) In the subsequent sums of Eq. A.5 and A.6, we choose $\mathbf{k}'+\rho=\mathbf{k}+\eta$ and $\mathbf{k}'+\gamma=\mathbf{k}+\mathbf{q}+\delta$ so that we get the additional restriction that, given $\rho,\eta,\ \gamma\in[-N\mathbf{q},N\mathbf{q}]\ s.t.\ |\rho-\eta-\mathbf{q}-\gamma|\leq N\mathbf{q}$. It turns out that choosing $N_{\mathbf{q}}$ in the order of ~ 10 provides reasonable convergence for the parameters presented in Table 3.1. However, this number rapidly increases with increasing pumping incident energy, as compared to the number of off-diagonal terms we needed in the previous formalism.

To limit the number of equations to a reasonable number, it is necessary to use a smaller intensity of pump than in the previous chapter. We also choose a smaller time-constant in order to decrease the length of the calculations as well. Nevertheless, we expect the same qualitative physics as we are still in the same non-adiabatic, small fluence regime as in the previous chapter. Moreover, similar modifications of the pump parameters in the previous formalism resulted in equivalent qualitative behaviour to the parameters used in Chapter 1 (Table 2.2). The parameters used here are presented in Table 3.1.

3.4.2 Nonequilibrium Green's functions

The solutions of the equations of motion can then be used to calculate all Green's function $G(k,t,t')$, which we want to relate to the ARPES spectra. Rewriting the operators in terms of the Bogoliubov quasiparticle operators,

$$\langle c_{\mathbf{k},\uparrow}(t),c^\dagger_{\mathbf{k},\uparrow}(t')\rangle=\langle(u_{\mathbf{k}}\alpha_{\mathbf{k}}(t)-v_{\mathbf{k}}\beta^\dagger_{\mathbf{k}}(t))(u_{\mathbf{k}}\alpha^\dagger_{\mathbf{k}}(t')-v_{\mathbf{k}}\beta_{\mathbf{k}}(t'))\rangle \tag{3.29a}$$

$$\langle c_{\mathbf{k},\downarrow}(t),c^\dagger_{\mathbf{k},\downarrow}(t')\rangle=\langle(v_{-\mathbf{k}}\alpha^\dagger_{-\mathbf{k}}(t)+v_{-\mathbf{k}}\beta_{-\mathbf{k}}(t))(v_{-\mathbf{k}}\alpha_{-\mathbf{k}}(t')+u_{-\mathbf{k}}\beta^\dagger_{-\mathbf{k}}(t'))\rangle. \tag{3.29b}$$

However, as our Hamiltonian is spin symmetric, it will suffice to consider only the spin-up regime.

Thus, for the non-equilibrium Green's functions,

$$G^{>}(\mathbf{k},t,t') = -i\langle(u_{\mathbf{k}}\alpha_{\mathbf{k}}(t) - v_{\mathbf{k}}\beta^{\dagger}_{\mathbf{k}}(t))(u_{\mathbf{k}}\alpha^{\dagger}_{\mathbf{k}}(t') - v_{\mathbf{k}}\beta_{\mathbf{k}}(t'))\rangle \tag{3.30a}$$

$$G^{<}(\mathbf{k},t,t') = +i\langle(u_{\mathbf{k}}\alpha^{\dagger}_{\mathbf{k}}(t') - v_{\mathbf{k}}\beta_{\mathbf{k}}(t'))(u_{\mathbf{k}}\alpha_{\mathbf{k}}(t) - v_{\mathbf{k}}\beta^{\dagger}_{\mathbf{k}}(t))\rangle. \tag{3.30b}$$

Finally, using Eqs. 3.21 and 3.23, in terms of the ansatz, the non-equillibrium Green's functions are,

$$\begin{aligned} &G^{>}(\mathbf{k},t,t') = \\ &\quad -i\sum_{\rho}\left[u^2_{\mathbf{k}}l^{*}_{\mathbf{k},\rho}(t)l_{\mathbf{k},\rho}(t') - v_{\mathbf{k}}u_{\mathbf{k}}o_{\mathbf{k},\rho}(t)l_{\mathbf{k},\rho}(t') - v_{\mathbf{k}}u_{\mathbf{k}}l^{*}_{\mathbf{k},\rho}(t)o^{*}_{\mathbf{k},\rho}(t') + v^2_{\mathbf{k}}o_{\mathbf{k},\rho}(t)o^{*}_{\mathbf{k},\rho}(t')\right] \end{aligned} \tag{3.31a}$$

$$\begin{aligned} &G^{<}(\mathbf{k},t,t') = \\ &\quad +i\sum_{\rho}\left[u^2_{\mathbf{k}}m_{\mathbf{k},\rho}(t')m^{*}_{\mathbf{k},\rho}(t) - v_{\mathbf{k}}u_{\mathbf{k}}m_{\mathbf{k},\rho}(t')n_{\mathbf{k},\rho}(t) - v_{\mathbf{k}}u_{\mathbf{k}}n^{*}_{\mathbf{k},\rho}(t')m^{*}_{\mathbf{k},\rho}(t) + v^2_{\mathbf{k}}n^{*}_{\mathbf{k},\rho}(t')n_{\mathbf{k},\rho}(t)\right] \end{aligned} \tag{3.31b}$$

and for the retarded and advanced Green's functions,

$$\begin{aligned} &G^{R}(\mathbf{k},t,t') = \\ &\quad \Theta(t-t')\sum_{\rho}\big[u^2_{\mathbf{k}}l^{*}_{\mathbf{k},\rho}(t)l_{\mathbf{k},\rho}(t') - v_{\mathbf{k}}u_{\mathbf{k}}o_{\mathbf{k},\rho}(t)l_{\mathbf{k},\rho}(t') - v_{\mathbf{k}}u_{\mathbf{k}}l^{*}_{\mathbf{k},\rho}(t)o^{*}_{\mathbf{k},\rho}(t') + v^2_{\mathbf{k}}o_{\mathbf{k},\rho}(t)o^{*}_{\mathbf{k},\rho}(t') \\ &\qquad - u^2_{\mathbf{k}}m_{\mathbf{k},\rho}(t')m^{*}_{\mathbf{k},\rho}(t) + v_{\mathbf{k}}u_{\mathbf{k}}m_{\mathbf{k},\rho}(t')n_{\mathbf{k},\rho}(t) + v_{\mathbf{k}}u_{\mathbf{k}}n^{*}_{\mathbf{k},\rho}(t')m^{*}_{\mathbf{k},\rho}(t) - v^2_{\mathbf{k}}n^{*}_{\mathbf{k},\rho}(t')n_{\mathbf{k},\rho}\big] \end{aligned} \tag{3.32a}$$

$$\begin{aligned} &G^{A}(\mathbf{k},t,t') = \\ &\quad \Theta(t'-t)\sum_{\rho}\big[-u^2_{\mathbf{k}}l^{*}_{\mathbf{k},\rho}(t)l_{\mathbf{k},\rho}(t') + v_{\mathbf{k}}u_{\mathbf{k}}o_{\mathbf{k},\rho}(t)l_{\mathbf{k},\rho}(t') + v_{\mathbf{k}}u_{\mathbf{k}}l^{*}_{\mathbf{k},\rho}(t)o^{*}_{\mathbf{k},\rho}(t') - v^2_{\mathbf{k}}o_{\mathbf{k},\rho}(t)o^{*}_{\mathbf{k},\rho}(t') \\ &\qquad + u^2_{\mathbf{k}}m_{\mathbf{k},\rho}(t')m^{*}_{\mathbf{k},\rho}(t) - v_{\mathbf{k}}u_{\mathbf{k}}m_{\mathbf{k},\rho}(t')n_{\mathbf{k},\rho}(t) - v_{\mathbf{k}}u_{\mathbf{k}}n^{*}_{\mathbf{k},\rho}(t')m^{*}_{\mathbf{k},\rho}(t) + v^2_{\mathbf{k}}n^{*}_{\mathbf{k},\rho}(t')n_{\mathbf{k},\rho}\big] \end{aligned} \tag{3.32b}$$

3.5 Results

3.5.1 Higgs oscillations

Similarly to the previous chapter, following the application of a pumping laser, the magnitude of the order parameter decreases and oscillates due to changes in the free energy potential of the superconductor. The degree to which the potential is altered again depends both on the amplitude and length of the pump. Since we are interested particularly in understanding the second Higgs mode in a $d_{x^2-y^2}$ superconductor, we will focus immediately on those results. The results for our specific parameters are presented in Fig. 3.1 and agree well with the results from the previous formalism (Fig. 2.3). There is once again a well-defined oscillation frequency at 2Δ and a second low-energy frequency below this threshold. This shows that our ansatz reproduces the same physics from the previous chapter.

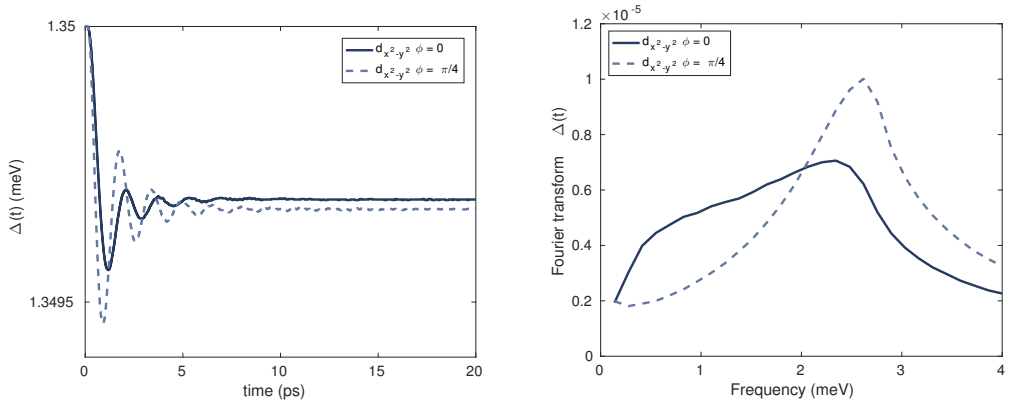

(a) (b)

Figure 3.1: (a) Absolute value of a $d_{x^2-y^2}$ order parameter $\Delta(t)$ as a function of time following the pump in the new formalism. (b) Fourier transform of the order parameter in (a). ϕ is the relative angle between the antinode of the $d_{x^2-y^2}$ order parameter and the direction of the vector potential of the pump.

3.5.2 Spectral Function

To determine the symmetry of the oscillations and thus, the order parameter, it is most useful to visualize the spectral function within the energy scale of the order parameter Δ. These results are presented in Fig. 3.2 after a time-delay of 0.55 picoseconds and for a pump polarized so that the vector potential lies along $\theta = \pi/2$ in the polar plots. The $d_{x^2-y^2}$ character is easily evident. However, for a vector potential aligned along the antinode (Fig. 3.2(a)), the $\hat{xy}$ intensity symmetry is broken between the $d_{x^2-y^2}$ nodes, along the C_2'' axis, which is indicative of the osculating, B1g nonequilibrium mode (Fig. 2.2 d). In contrast, when the vector potential is aligned along the node (Fig. 3.2(b)), the symmetry between antinodes is not broken. Rather, the C_2' symmetry is broken within a single antinode. Together, these facts point towards the second Higgs oscillation mode coming from an osculating origin.

This symmetry breaking is further exemplified when looking at the time-delay data for various points around the Fermi surface and near to the antinode. In Fig. 3.3, we show the oscillations in the spectral function as a function of time-delay. Notably, the oscillations of the spectral function are fixed in energy and only the amplitude oscillates in our calculations. These oscillations again have characteristic frequencies corresponding to the two modes in Fig. 3.1. For the vector potential aligned along the antinode (Fig. 3.3(a)), there is a single sharp peak at $\Delta(\theta)$ for angles away from the $\theta = \pi/2$ ($\theta = 3\pi/2$) antinode. However, near to this antinode, the peak becomes broad and an additional peak is clearly visible in the spectral function at the antinode. In contrast, for a vector potential aligned along the node (Fig. 3.3(b)), while there is broadening along the $\theta = \pi/2$ direction, there is no additional peak in the spectral function along a specific antinodes or antinodes.

3.6 Discussion

The ansatz proposed in this section is clearly a powerful tool for determining additional information beyond what can be achieved by the density matrix formalism, while still maintaining the same

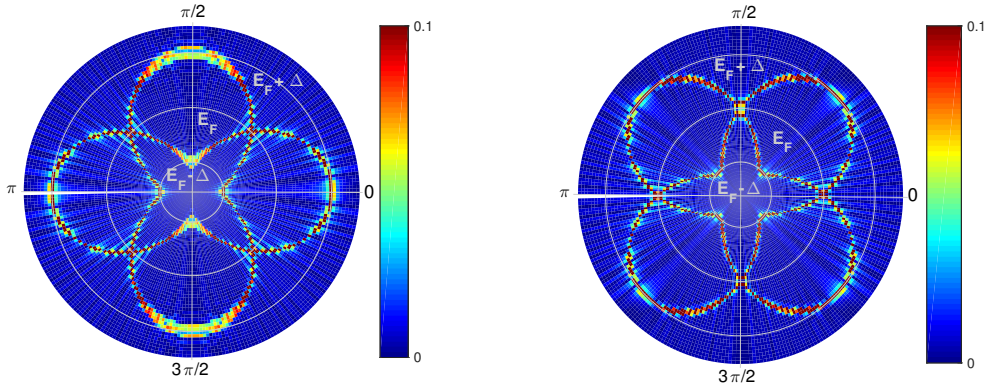

(a) (b)

Figure 3.2: Comparison of the spectral functions $A(\theta, \omega)$ for a pumped $d_{x^2-y^2}$ superconductor after 0.55 picoseconds, with the vector potential aligned (a) vertically along the antinode (b) vertically along the node.

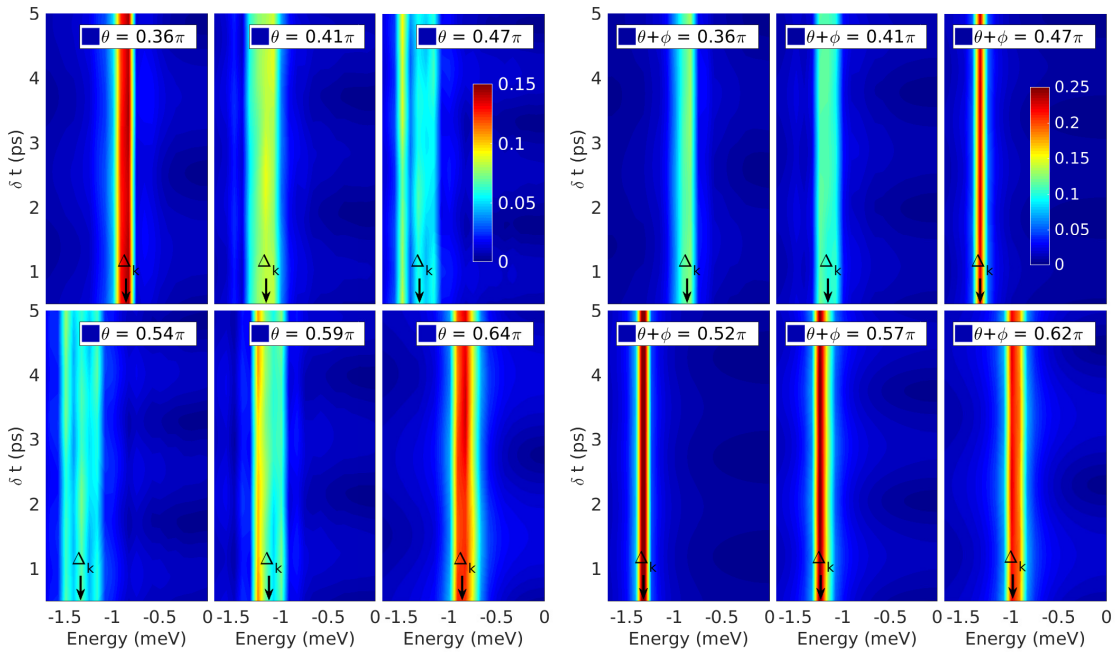

(a) (b)

Figure 3.3: Comparison of the spectral functions $A(\theta, \omega, \delta t)$ near the antinode for a pumped $d_{x^2-y^2}$ superconductor with the vector potential lying along the (a) antinode and (b) node, as a function of delay-time δt. The plots correspond to various polar angle cuts near to the $\pi/2$ antinode in Fig. 3.2(a) and the $3\pi/4$ antinode in Fig. 3.2(b).

underlying physics. In our model, we are able to use this ansatz to reproduce the spectral function for a superconductor with arbitrary symmetry interacting with an electromagnetic field and predict the ARPES response based on the nonequilibrium spectral function. Having this information is particularly useful for evaluating the symmetry-breaking terms since ARPES (and the spectral function) contain relevant experimental momentum information, which is integrated over in optical experiments simulated in the previous chapter on optical response.

Considering the group symmetry of our lattice, we know the oscillations must fall into the category of either the A1g, A2g, B2g or B1g symmetries. We can now identify the mode at 2Δ as the A1g, or breathing mode from our analysis in the previous chapter and comparisons with isotropic superconductors. In the spectral function, as the vector potential of the pump is aligned along the $d_{x^2-y^2}$ antinode there is a broken $\hat{xy}$ symmetry. That is, the C_4 and the C_2'' symmetry are broken, while the C_2' is not. This is more clear upon examination of the electromagnetic coupling term. While the second order term does not couple to the momentum, the first order term does couple to the $\hat{y}$ momentum along the direction of polarization, which breaks the C_2' momentum symmetry of the lattice. Accordingly, this shows that our second mode corresponds to the osculating mode in Fig. 2.2. In terms of the D_4 character table, the coupling to our electromagnetic field, which has been polarized such that the vector potential lies along the $\hat{y}$ axis, perturbs the equilibrium BCS Hamiltonian with a momentum anisotropy that is of A1g and B1g character.

For a pump polarization where the vector potential lies along the nodal direction, the C_2'' ($\hat{xy}$) symmetry is not broken. Instead, the C_2' symmetry is broken due to the $\pi/4$ sample rotation. However, there is no clear indication of a B2g mode as would be the case for this symmetry breaking. This should be somewhat expected because the pump should not induce any modes associated with an angular momentum symmetry breaking, as is the case of the A2g and B2g modes. Moreover, the momentum that incurs the maximum symmetry-breaking is along the nodal lines, which presents a further explanation regarding the absence of this mode in the superconducting amplitude Higgs mode oscillations.

Chapter 4

Conclusions and Outlook

The subject of this thesis is the nonequilibrium response of superconductors with different pairing symmetries. The experimentally motivated models studied in this thesis have revolved around the interaction of a BCS superconductor with a short-time electromagnetic field, modeled so as to emulate real experimental pump-probe spectroscopy. Our main findings show how this novel technique, Higgs spectroscopy, can be used both to excite and study the nonequilibrium superconducting mode(s), as well as distinguish and study the inherent superconducting symmetries of the system in various experimental setups.

In chapter 2, we used two short-time electromagnetic fields to emulate the pump and probe respectively. We found that the first interaction with the electromagnetic field (the pump) first reduced the size of the order parameter and then induced Higgs oscillations of the order parameter. As discussed in section 2.1, the change in value and the oscillations can be attributed to nonadiabatic changes to the free energy potential of the superconductor. An isotropic nonequilibrium oscillating mode at 2Δ was present regardless of the superconducting symmetry while a second lower energy mode appeared for a $d_{x^2-y^2}$, anisotropic superconductor depending on the relative orientation of the sample and polarization of the pump. In addition, a second short-time electromagnetic interaction was included to simulate an experimental probing pulse after some time-delay. With this second pulse, we can calculate the optical response (conductivity) of the system. For a $d_{x^2-y^2}$ superconductor, we can then isolate the two different responses by either orienting the vector potential along a $d_{x^2-y^2}$ antinode to induce only the low energy mode, or along the $d_{x^2-y^2}$ node to induce only the 2Δ mode. As a function of delay-time, the conductivity also exhibited oscillations in amplitude with both the low energy and 2Δ frequencies. Overall, we showed how an optical experiment can be used to measure various symmetry-dependent nonequilibrium Higgs modes and actually resolve the momentum pairing symmetry of a superconductor.

In chapter 3, we first developed a formalism to study the spectral function and determine the two-time Green's functions for a superconductor interacting with an electromagnetic field. This framework allowed us to additionally make predictions regarding the time-resolved ARPES (tr-ARPES) response. The results from our approximation compare well with the results from the more established density matrix formalism in chapter 2 and we were able to reproduce the same angle-dependent Higgs modes for a $d_{x^2-y^2}$ superconductor. Moreover, this new formalism allowed us to study the momentum dependence of the time-resolved response. Particularly, we were able to identify that a vector potential aligned along one of the antinodes of a $d_{x^2-y^2}$ superconductor induced an $\hat{x}-\hat{y}$ symmetry breaking, which is characteristic of the osculating nonequilibrium mode of a $d_{x^2-y^2}$ superconductor. In contrast, a vector potential aligned alone one of the nodes of a $d_{x^2-y^2}$ superconductor did not induce the same symmetry breaking. From this, we were able to posit that the low energy Higgs mode, generated by pumping with a vector potential aligned along the $d_{x^2-y^2}$ antinode, corresponds to the osculating nonequilibrium Higgs mode and that the 2Δ mode,

which can be seen regardless of the polarization or superconductor symmetry, corresponds to the isotropic breathing mode. Thus, beyond already being able to identify aspects of the superconducting symmetry in equilibrium, utilizing momentum and time-resolved experimental techniques, such as tr-ARPES, is crucial to experimentally verifying the exact momentum-dependent nature of the nonequilibrium Higgs oscillations in a superconductor.

Higgs spectroscopy presents a novel experimental technique for directly probing and studying properties of the superconducting condensate regardless of the pairing symmetry. One of the most promising extensions of this work would be to exploit the coupling between the pump and the superconducting momentum by applying series of ultra-fast pumps with different geometry to excite angular momentum-dependent modes or study the effects of depopulating electron-pairs along particular momenta and breaking the superconducting symmetry along different axes. The methods in this thesis can easily be extended to study other superconducting symmetries than considered here, such as p-wave and anisotropic s-wave. In addition, the methods can also be used to study the phase of the superconducting condensate and phase-dependent nonequilibrium response, which can be a powerful tool for determining the phase differences present in s$\pm$ superconductors. As an experimental technique, with refinement and experience, Higgs spectroscopy will likely uncover more physics beyond the scope of this thesis.

In conclusion, the novel field of Higgs spectroscopy is just emerging. In this thesis, we have developed a theoretical framework to describe the nonequilibrium Higgs mode, as well as proposed the experimental setups that would be required to excite different symmetry dependent nonequilibrium Higgs modes in both optical and time-resolved ARPES experiments. These methods can sequentially resolve the symmetry-dependent response, which can be used to both resolve the different pairing symmetries, as well as the inherent symmetry in the different Higgs amplitude modes.

Bibliography

[1] J. Bardeen. Theory of the meissner effect in superconductors. *Phys. Rev.*, 97:1724–1725, Mar 1955.

[2] J. Bardeen, L. N. Cooper, and J. R. Schrieffer. Microscopic theory of superconductivity. *Phys. Rev.*, 106:162–164, Apr 1957.

[3] J. Bardeen, L. N. Cooper, and J. R. Schrieffer. Theory of superconductivity. *Phys. Rev.*, 108:1175–1204, Dec 1957.

[4] Yafis Barlas and C. M. Varma. Amplitude or higgs modes in d-wave superconductors. *Physical Review B*, 87(5), feb 2013.

[5] M. Beck, M. Klammer, S. Lang, P. Leiderer, V. V. Kabanov, G. N. Gol'tsman, and J. Demsar. Energy-gap dynamics of superconducting nbn thin films studied by time-resolved terahertz spectroscopy. *Phys. Rev. Lett.*, 107:177007, Oct 2011.

[6] M. Beck, I. Rousseau, M. Klammer, P. Leiderer, M. Mittendorff, S. Winnerl, M. Helm, G. N. Gol'tsman, and J. Demsar. Transient increase of the energy gap of superconducting nbn thin films excited by resonant narrow-band terahertz pulses. *Phys. Rev. Lett.*, 110:267003, Jun 2013.

[7] J. G. Bednorz and K. A. Müller. Possible high T_c superconductivity in the Ba-La-Cu-O system. *Zeitschrift für Physik B Condensed Matter*, 64(2):189–193, jun 1986.

[8] T. Cea, C. Castellani, and L. Benfatto. Nonlinear optical effects and third-harmonic generation in superconductors: Cooper pairs versus higgs mode contribution. *Phys. Rev. B*, 93:180507, May 2016.

[9] Yang-Zhi Chou, Yunxiang Liao, and Matthew S. Foster. Twisting anderson pseudospins with light: Quench dynamics in terahertz-pumped bcs superconductors. *Phys. Rev. B*, 95:104507, Mar 2017.

[10] S. Dal Conte, C. Giannetti, G. Coslovich, F. Cilento, D. Bossini, T. Abebaw, F. Banfi, G. Ferrini, H. Eisaki, M. Greven, A. Damascelli, D. van der Marel, and F. Parmigiani. Disentangling the electronic and phononic glue in a high-tc superconductor. *Science*, 335(6076):1600–1603, mar 2012.

[11] Leon N. Cooper. Bound electron pairs in a degenerate fermi gas. *Phys. Rev.*, 104:1189–1190, Nov 1956.

[12] Andrea Damascelli, Zahid Hussain, and Zhi-Xun Shen. Angle-resolved photoemission studies of the cuprate superconductors. *Rev. Mod. Phys.*, 75:473–541, Apr 2003.

[13] Thomas P. Devereaux and Rudi Hackl. Inelastic light scattering from correlated electrons. *Rev. Mod. Phys.*, 79:175–233, Jan 2007.

[14] M.S. Dresselhaus, G. Dresselhaus, and A. Jorio. *Group Theory: Application to the Physics of Condensed Matter*. SpringerLink: Springer e-Books. Springer Berlin Heidelberg, 2007.

[15] Maxim Dzero, Maxim Khodas, and Alex Levchenko. Amplitude modes and dynamic coexistence of competing orders in multicomponent superconductors. *Phys. Rev. B*, 91:214505, Jun 2015.

[16] B. Fauseweh, L. Schwarz, N. Tsuji, N. Cheng, N. Bittner, H. Krull, M. Berciu, G. S. Uhrig, A. P. Schnyder, S. Kaiser, and D. Manske. Higgs spectroscopy of superconductors in nonequilibrium. *ArXiv e-prints*, December 2017.

[17] J. K. Freericks, H. R. Krishnamurthy, and Th. Pruschke. Theoretical description of time-resolved photoemission spectroscopy: Application to pump-probe experiments. *Physical Review Letters*, 102(13), mar 2009.

[18] Vitaly L. Ginzburg. On superconductivity and superfluidity (what i have and have not managed to do), as well as on the'physical minimum' at the beginning of the 21st century. *ChemPhysChem*, 5(7):930–945, jul 2004.

[19] Simone A. Hamerla and Götz S. Uhrig. Dynamical transition in interaction quenches of the one-dimensional hubbard model. *Physical Review B*, 87(6), feb 2013.

[20] Simone A Hamerla and Götz S Uhrig. One-dimensional fermionic systems after interaction quenches and their description by bosonic field theories. *New Journal of Physics*, 15(7):073012, jul 2013.

[21] Simone A. Hamerla and Götz S. Uhrig. Interaction quenches in the two-dimensional fermionic hubbard model. *Phys. Rev. B*, 89:104301, Mar 2014.

[22] Peter W. Higgs. Broken symmetries and the masses of gauge bosons. *Physical Review Letters*, 13(16):508–509, oct 1964.

[23] Stefan Kaiser. Light-induced superconductivity in high-tc cuprates. *Physica Scripta*, 92(10):103001, aug 2017.

[24] Kota Katsumi, Naoto Tsuji, Yuki I. Hamada, Ryusuke Matsunaga, John Schneeloch, Ruidan D. Zhong, Genda D. Gu, Hideo Aoki, Yann Gallais, and Ryo Shimano. Higgs mode in the d -wave superconductor bi2sr2cacu2o8+x driven by an intense terahertz pulse. *Physical Review Letters*, 120(11), mar 2018.

[25] A. F. Kemper, M. A. Sentef, B. Moritz, J. K. Freericks, and T. P. Devereaux. Direct observation of higgs mode oscillations in the pump-probe photoemission spectra of electron-phonon mediated superconductors. *Phys. Rev. B*, 92:224517, Dec 2015.

[26] H. Krull, N. Bittner, G. S. Uhrig, D. Manske, and A. P. Schnyder. Coupling of higgs and leggett modes in non-equilibrium superconductors. *Nature Communications*, 7:11921, jun 2016.

[27] H. Krull, D. Manske, G. S. Uhrig, and A. P. Schnyder. Signatures of nonadiabatic bcs state dynamics in pump-probe conductivity. *Phys. Rev. B*, 90:014515, Jul 2014.

[28] L.D. Landau and E.M. Lifshitz. *Statistical Physics*. Number 5 in v. Elsevier Science, 2013.

[29] Ryusuke Matsunaga, Yuki I. Hamada, Kazumasa Makise, Yoshinori Uzawa, Hirotaka Terai, Zhen Wang, and Ryo Shimano. Higgs amplitude mode in the bcs superconductors $nb_{1-x}ti_x\mathbf{N}$ induced by terahertz pulse excitation. *Phys. Rev. Lett.*, 111:057002, Jul 2013.

[30] Ryusuke Matsunaga and Ryo Shimano. Nonequilibrium bcs state dynamics induced by intense terahertz pulses in a superconducting nbn film. *Phys. Rev. Lett.*, 109:187002, Oct 2012.

[31] Ryusuke Matsunaga, Naoto Tsuji, Hiroyuki Fujita, Arata Sugioka, Kazumasa Makise, Yoshinori Uzawa, Hirotaka Terai, Zhen Wang, Hideo Aoki, and Ryo Shimano. Light-induced collective pseudospin precession resonating with higgs mode in a superconductor. *Science*, 345(6201):1145–1149, 2014.

[32] Ryusuke Matsunaga, Naoto Tsuji, Kazumasa Makise, Hirotaka Terai, Hideo Aoki, and Ryo Shimano. Polarization-resolved terahertz third-harmonic generation in a single-crystal superconductor nbn: Dominance of the higgs mode beyond the bcs approximation. *Phys. Rev. B*, 96:020505, Jul 2017.

[33] M. Mitrano, A. Cantaluppi, D. Nicoletti, S. Kaiser, A. Perucchi, S. Lupi, P. Di Pietro, D. Pontiroli, M. Riccò, S. R. Clark, D. Jaksch, and A. Cavalleri. Possible light-induced superconductivity in k3c60 at high temperature. *Nature*, 530(7591):461–464, feb 2016.

[34] Yuta Murakami, Philipp Werner, Naoto Tsuji, and Hideo Aoki. Damping of the collective amplitude mode in superconductors with strong electron-phonon coupling. *Phys. Rev. B*, 94:115126, Sep 2016.

[35] Yuta Murakami, Philipp Werner, Naoto Tsuji, and Hideo Aoki. Multiple amplitude modes in strongly coupled phonon-mediated superconductors. *Phys. Rev. B*, 93:094509, Mar 2016.

[36] B. Nosarzewski, B. Moritz, J. K. Freericks, A. F. Kemper, and T. P. Devereaux. Amplitude mode oscillations in pump-probe photoemission spectra from a d -wave superconductor. *Physical Review B*, 96(18), nov 2017.

[37] T. Papenkort, V. M. Axt, and T. Kuhn. Coherent dynamics and pump-probe spectra of bcs superconductors. *Phys. Rev. B*, 76:224522, Dec 2007.

[38] T. Papenkort, T. Kuhn, and V. M. Axt. Coherent control of the gap dynamics of bcs superconductors in the nonadiabatic regime. *Phys. Rev. B*, 78:132505, Oct 2008.

[39] A. Pashkin and A. Leitenstorfer. Particle physics in a superconductor. *Science*, 345(6201):1121–1122, sep 2014.

[40] A. Pashkin, M. Porer, M. Beyer, K. W. Kim, A. Dubroka, C. Bernhard, X. Yao, Y. Dagan, R. Hackl, A. Erb, J. Demsar, R. Huber, and A. Leitenstorfer. Femtosecond response of quasiparticles and phonons in superconducting $yba_2cu_3\mathbf{o}_{7-\delta}$ studied by wideband terahertz spectroscopy. *Phys. Rev. Lett.*, 105:067001, Aug 2010.

[41] David Pekker and C.M. Varma. Amplitude/higgs modes in condensed matter physics. *Annual Review of Condensed Matter Physics*, 6(1):269–297, mar 2015.

[42] Francesco Peronaci, Marco Schiró, and Massimo Capone. Transient dynamics of d-wave superconductors after a sudden excitation. *Phys. Rev. Lett.*, 115:257001, Dec 2015.

[43] Daniel Podolsky, Assa Auerbach, and Daniel P. Arovas. Visibility of the amplitude (higgs) mode in condensed matter. *Physical Review B*, 84(17), nov 2011.

[44] Andreas P. Schnyder, Dirk Manske, and Adolfo Avella. Resonant generation of coherent phonons in a superconductor by ultrafast optical pump pulses. *Phys. Rev. B*, 84:214513, Dec 2011.

[45] Daniel Sherman, Uwe S. Pracht, Boris Gorshunov, Shachaf Poran, John Jesudasan, Madhavi Chand, Pratap Raychaudhuri, Mason Swanson, Nandini Trivedi, Assa Auerbach, Marc Scheffler, Aviad Frydman, and Martin Dressel. The higgs mode in disordered superconductors close to a quantum phase transition. *Nature Physics*, 11(2):188–192, jan 2015.

[46] R. Sooryakumar and M. V. Klein. Raman scattering by superconducting-gap excitations and their coupling to charge-density waves. *Phys. Rev. Lett.*, 45:660–662, Aug 1980.

[47] Sofia-Michaela Souliou, Jiří Chaloupka, Giniyat Khaliullin, Gihun Ryu, Anil Jain, B. J. Kim, Matthieu Le Tacon, and Bernhard Keimer. Raman scattering from higgs mode oscillations in the two-dimensional antiferromagnet ca2ruo4. *Physical Review Letters*, 119(6), aug 2017.

[48] Naoto Tsuji and Hideo Aoki. Theory of anderson pseudospin resonance with higgs mode in superconductors. *Phys. Rev. B*, 92:064508, Aug 2015.

[49] Naoto Tsuji, Yuta Murakami, and Hideo Aoki. Nonlinear light˘higgs coupling in superconductors beyond bcs: Effects of the retarded phonon-mediated interaction. *Phys. Rev. B*, 94:224519, Dec 2016.

[50] J. Unterhinninghofen, D. Manske, and A. Knorr. Theory of ultrafast nonequilibrium dynamics in d-wave superconductors. *Phys. Rev. B*, 77:180509, May 2008.

[51] Dirk van Delft and Peter Kes. The discovery of superconductivity. *Physics Today*, 63(9):38–43, sep 2010.

[52] Emil A. Yuzbashyan, Boris L. Altshuler, Vadim B. Kuznetsov, and Victor Z. Enolskii. Nonequilibrium cooper pairing in the nonadiabatic regime. *Phys. Rev. B*, 72:220503, Dec 2005.

[53] Emil A. Yuzbashyan, Oleksandr Tsyplyatyev, and Boris L. Altshuler. Erratum: Relaxation and persistent oscillations of the order parameter in fermionic condensates [phys. rev. lett. **96** , 097005 (2006)]. *Phys. Rev. Lett.*, 96:179905, May 2006.

Appendix A

First Appendix

The full derivation of the equations of motion for the operators in Chapter 3 are presented here. Beginning with $\alpha^{\dagger}_{\mathbf{k}'}$ and the commutator with the superconducting portion of the Hamiltonian (the time-dependence of the pre-factors l, m, n and o is taken to be implicit for simplified notation),

$$
\begin{aligned}
&\left[\alpha^{\dagger}_{\mathbf{k}'}(t),\ \ \tilde{H}_{sc}\right] \\
&= \sum_{\mathbf{k},\delta,\eta,\gamma} \Bigg[\alpha^{\dagger}_{\mathbf{k}+\delta}(-\delta_{\mathbf{k}'+\gamma,\mathbf{k}+\eta}) \Big(l_{\mathbf{k}',\gamma} \Big((l_{\mathbf{k},\delta} l^{*}_{\mathbf{k},\eta} - o^{*}_{\mathbf{k},\delta} o_{\mathbf{k},\eta}) R_{\mathbf{k}} + (l_{\mathbf{k},\delta} o_{\mathbf{k},\eta}) C_{\mathbf{k}} + (l^{*}_{\mathbf{k},\eta} o^{*}_{\mathbf{k},\delta}) C^{*}_{\mathbf{k}} \Big) \\
&\qquad\qquad + m_{\mathbf{k}',\gamma} \Big((l_{\mathbf{k}-\delta} m^{*}_{\mathbf{k},\eta} + n_{\mathbf{k},\eta} o^{*}_{\mathbf{k},\delta}) R_{\mathbf{k}} + (l_{\mathbf{k},\delta} n_{\mathbf{k},\eta}) C_{\mathbf{k}} + (o^{*}_{\mathbf{k},\delta} m^{*}_{\mathbf{k},\eta}) C^{*}_{\mathbf{k}} \Big) \Big) \\
&\qquad + \beta_{\mathbf{k}+\delta}(\delta_{\mathbf{k}'+\gamma,\mathbf{k}+\eta}) \Big(m_{\mathbf{k}',\gamma} \Big((-m^{*}_{\mathbf{k},\eta} m_{\mathbf{k},\delta} + n_{\mathbf{k},\eta} n^{*}_{\mathbf{k},\delta}) R_{\mathbf{k}} + (-m_{\mathbf{k},\delta} n_{\mathbf{k},\eta}) C_{\mathbf{k}} - (m^{*}_{\mathbf{k},\eta} n^{*}_{\mathbf{k},\delta}) C^{*}_{\mathbf{k}} \Big) \\
&\qquad\qquad - l_{\mathbf{k}',\gamma} \Big((m_{\mathbf{k},\delta} l^{*}_{\mathbf{k},\eta} - n^{*}_{\mathbf{k},\delta} o_{\mathbf{k},\eta}) R_{\mathbf{k}} + (m_{\mathbf{k},\delta} o_{\mathbf{k},\eta}) C_{\mathbf{k}} + (n^{*}_{\mathbf{k},\delta} l^{*}_{\mathbf{k},\eta}) C^{*}_{\mathbf{k}} \Big) \Big) \Bigg]
\end{aligned}
\tag{A.1}
$$

and for $\beta^{\dagger}_{\mathbf{k}}$ and the commutator with the superconducting portion of the Hamiltonian,

$$
\begin{aligned}
&\left[\beta^{\dagger}_{\mathbf{k}'}(t),\ \ \tilde{H}_{sc}\right] \\
&= \sum_{\mathbf{k},\delta,\eta,\gamma} \Bigg[\alpha_{\mathbf{k}+\eta}(\delta_{\mathbf{k}'+\gamma,\mathbf{k}+\delta}) \Big(o_{\mathbf{k}',\gamma} \Big((l_{\mathbf{k},\delta} l^{*}_{\mathbf{k},\eta} - o^{*}_{\mathbf{k},\delta} o_{\mathbf{k},\eta}) R_{\mathbf{k}} + (l_{\mathbf{k},\delta} o_{\mathbf{k},\eta}) C_{\mathbf{k}} + (l^{*}_{\mathbf{k},\eta} o^{*}_{\mathbf{k},\delta}) C^{*}_{\mathbf{k}} \Big) \\
&\qquad\qquad + n_{\mathbf{k}',\gamma} \Big((m_{\mathbf{k},\delta} l^{*}_{\mathbf{k},\eta} - n^{*}_{\mathbf{k},\delta} o_{\mathbf{k},\eta}) R_{\mathbf{k}} + (m_{\mathbf{k},\delta} o_{\mathbf{k},\eta}) C_{\mathbf{k}} + (n^{*}_{\mathbf{k},\delta} l^{*}_{\mathbf{k},\eta}) C^{*}_{\mathbf{k}} \Big) \Big) \\
&\qquad + \beta^{\dagger}_{\mathbf{k}+\eta}(\delta_{\mathbf{k}'+\gamma,\mathbf{k}+\delta}) \Big(-n_{\mathbf{k}',\gamma} \Big((-m^{*}_{\mathbf{k},\eta} m_{\mathbf{k},\delta} + n_{\mathbf{k},\eta} n^{*}_{\mathbf{k},\delta}) R_{\mathbf{k}} + (-m_{\mathbf{k},\delta} n_{\mathbf{k},\eta}) C_{\mathbf{k}} - (m^{*}_{\mathbf{k},\eta} n^{*}_{\mathbf{k},\delta}) C^{*}_{\mathbf{k}} \Big) \\
&\qquad\qquad + o_{\mathbf{k}',\gamma} \Big((l_{\mathbf{k},\delta} m^{*}_{\mathbf{k},\eta} - n_{\mathbf{k},\eta} o^{*}_{\mathbf{k},\delta}) R_{\mathbf{k}} + (l_{\mathbf{k},\delta} n_{\mathbf{k},\eta}) C_{\mathbf{k}} + (o^{*}_{\mathbf{k},\delta} m^{*}_{\mathbf{k},\eta}) C^{*}_{\mathbf{k}} \Big) \Big) \Bigg]
\end{aligned}
\tag{A.2}
$$

and for $\beta^{\dagger}_{\mathbf{k}}$ and the commutator with the EM portion of the Hamiltonian,

$$
\begin{aligned}
&\left[\beta^{\dagger}_{\mathbf{k}'}(t), \tilde{H}_{em}\right] \\
&\quad = \left[\frac{e\hbar}{2m}\sum_{\mathbf{k},\mathbf{q},\delta,\eta,\gamma}(2\mathbf{k}+\mathbf{q})A_{\mathbf{q}}\right]\times \\
&\Bigg[\alpha_{\mathbf{k}+\eta}(\delta_{\mathbf{k}'+\gamma,\mathbf{k}+\delta+\mathbf{q}})\Big(o_{\mathbf{k}',\gamma}\Big((l_{\mathbf{k}+\mathbf{q},\delta}l^{*}_{\mathbf{k},\eta}+o^{*}_{\mathbf{k}+\mathbf{q},\delta}o_{\mathbf{k},\eta})L^{+}_{\mathbf{k},\mathbf{q}}+(-l_{\mathbf{k}+\mathbf{q},\delta}o_{\mathbf{k},\eta}+o^{*}_{\mathbf{k}+\mathbf{q},\delta}l^{*}_{\mathbf{k},\eta})M^{-}_{\mathbf{k},\mathbf{q}}\Big) \\
&\qquad\qquad + n_{\mathbf{k}',\gamma}\Big((m_{\mathbf{k}+\mathbf{q},\delta}l^{*}_{\mathbf{k},\eta}+n^{*}_{\mathbf{k}+\mathbf{q},\delta}o_{\mathbf{k},\eta})L^{+}_{\mathbf{k}.\mathbf{q}}+(-m_{\mathbf{k}+\mathbf{q},\delta}o_{\mathbf{k},\eta}+n^{*}_{\mathbf{k}+\mathbf{q},\delta}l^{*}_{\mathbf{k},\eta})M^{-}_{\mathbf{k},\mathbf{q}}\Big)\Big) \\
&+\beta^{\dagger}_{\mathbf{k}+\eta}(\delta_{\mathbf{k}'+\gamma,\mathbf{k}+\delta+\mathbf{q}})\quad\Big(-n_{\mathbf{k}',\gamma}\Big((-m^{*}_{\mathbf{k},\eta}m_{\mathbf{k}+\mathbf{q},\delta}-n_{\mathbf{k},\eta}n^{*}_{\mathbf{k}+\mathbf{q},\delta})L^{+}_{\mathbf{k},\mathbf{q}}+(+m_{\mathbf{k}+\mathbf{q},\delta}n_{\mathbf{k},\eta}-n^{*}_{\mathbf{k}+\mathbf{q},\delta}m^{*}_{\mathbf{k},\eta})M^{-}_{\mathbf{k},\mathbf{q}}\Big) \\
&\qquad\qquad + o_{\mathbf{k}',\gamma}\Big((l_{\mathbf{k}+\mathbf{q},\delta}m^{*}_{\mathbf{k},\eta}+n_{\mathbf{k},\eta}o^{*}_{\mathbf{k}+\mathbf{q},\delta})L^{+}_{\mathbf{k},\mathbf{q}}+(-l_{\mathbf{k}+\mathbf{q},\delta}n_{\mathbf{k},\eta}+o^{*}_{\mathbf{k}+\mathbf{q},\delta}m^{*}_{\mathbf{k},\eta})M^{-}_{\mathbf{k},\mathbf{q}}\Big)\Big)\Bigg] \\
&\quad + \left[\frac{e^2}{2m}\sum_{\mathbf{k},\mathbf{q},\delta,\eta,\gamma}\Big(\sum_{\mathbf{q}'}A_{\mathbf{q}-\mathbf{q}'}\cdot A_{\mathbf{q}'}\Big)\right]\times \\
&\Bigg[\alpha_{\mathbf{k}+\eta}(\delta_{\mathbf{k}'+\gamma,\mathbf{k}+\delta+\mathbf{q}})\Big(o_{\mathbf{k}',\gamma}\Big((l_{\mathbf{k}+\mathbf{q},\delta}l^{*}_{\mathbf{k},\eta}-o^{*}_{\mathbf{k}+\mathbf{q},\delta}o_{\mathbf{k},\eta})L^{-}_{\mathbf{k},\mathbf{q}}-(l_{\mathbf{k}+\mathbf{q},\delta}o_{\mathbf{k},\eta}+o^{*}_{\mathbf{k}+\mathbf{q},\delta}l^{*}_{\mathbf{k},\eta})M^{+}_{\mathbf{k},\mathbf{q}}\Big) \\
&\qquad\qquad + n_{\mathbf{k}',\gamma}\Big((m_{\mathbf{k}+\mathbf{q},\delta}l^{*}_{\mathbf{k},\eta}-n^{*}_{\mathbf{k}+\mathbf{q},\delta}o_{\mathbf{k},\eta})L^{-}_{\mathbf{k}.\mathbf{q}}-(m_{\mathbf{k}+\mathbf{q},\delta}o_{\mathbf{k},\eta}+n^{*}_{\mathbf{k}+\mathbf{q},\delta}l^{*}_{\mathbf{k},\eta})M^{+}_{\mathbf{k},\mathbf{q}}\Big)\Big) \\
&+\beta^{\dagger}_{\mathbf{k}+\eta}(\delta_{\mathbf{k}'+\gamma,\mathbf{k}+\delta+\mathbf{q}})\quad\Big(-n_{\mathbf{k}',\gamma}\Big((-m^{*}_{\mathbf{k},\eta}m_{\mathbf{k}+\mathbf{q},\delta}+n_{\mathbf{k},\eta}n^{*}_{\mathbf{k}+\mathbf{q},\delta})L^{-}_{\mathbf{k},\mathbf{q}}-(-m_{\mathbf{k}+\mathbf{q},\delta}n_{\mathbf{k},\eta}-n^{*}_{\mathbf{k}+\mathbf{q},\delta}m^{*}_{\mathbf{k},\eta})M^{+}_{\mathbf{k},\mathbf{q}}\Big) \\
&\qquad\qquad + o_{\mathbf{k}',\gamma}\Big((l_{\mathbf{k}+\mathbf{q},\delta}m^{*}_{\mathbf{k},\eta}-n_{\mathbf{k},\eta}o^{*}_{\mathbf{k}+\mathbf{q},\delta})L^{-}_{\mathbf{k},\mathbf{q}}-(l_{\mathbf{k}+\mathbf{q},\delta}n_{\mathbf{k},\eta}+o^{*}_{\mathbf{k}+\mathbf{q},\delta}m^{*}_{\mathbf{k},\eta})M^{+}_{\mathbf{k},\mathbf{q}}\Big)\Big)\Bigg]
\end{aligned}
\tag{A.3}
$$

and for $\beta_{\mathbf{k}'}$ with $\mathbf{k}'+\rho=\mathbf{k}+\delta$ in the first sum and $\mathbf{k}'=\mathbf{k}+\mathbf{q}+\delta$ in the subsequent 2 sums:

$$
\begin{aligned}
&i\hbar\frac{d}{dt}m_{\mathbf{k}',\rho}(t)\beta_{\mathbf{k}'+\rho} = \\
&-\sum_{\delta,\gamma}\beta_{\mathbf{k}'+\rho}\Big(m_{\mathbf{k}',\gamma}\Big((m^{*}_{\mathbf{k}'+\rho-\delta,\gamma+\delta-\rho}m_{\mathbf{k}'+\rho-\delta,\delta}-n_{\mathbf{k}'+\rho-\delta,\gamma+\delta-\rho}n^{*}_{\mathbf{k}'+\rho-\delta,\delta})R_{\mathbf{k}'+\rho-\delta}\\
&\qquad\qquad+(m_{\mathbf{k}'+\rho-\delta,\delta}n_{\mathbf{k}'+\rho-\delta,\gamma+\delta-\rho})C_{\mathbf{k}'+\rho-\delta}+(m^{*}_{\mathbf{k}'+\rho-\delta,\gamma+\delta-\rho}n^{*}_{\mathbf{k}'+\rho-\delta,\delta})C^{*}_{\mathbf{k}'+\rho-\delta}\Big)\\
&\qquad+l_{\mathbf{k}',\gamma}\Big((m_{\mathbf{k}'+\rho-\delta,\delta}l^{*}_{\mathbf{k}'+\rho-\delta,\gamma+\delta-\rho}-n^{*}_{\mathbf{k}'+\rho-\delta,\delta}o_{\mathbf{k}'+\rho-\delta,\gamma+\delta-\rho})R_{\mathbf{k}'+\rho-\delta}\\
&\qquad\qquad+(m_{\mathbf{k}'+\rho-\delta,\delta}o_{\mathbf{k}'+\rho-\delta,\gamma+\delta-\rho})C_{\mathbf{k}'+\rho-\delta}+(n^{*}_{\mathbf{k}'+\rho-\delta,\delta}l^{*}_{\mathbf{k}'+\rho-\delta,\gamma+\delta-\rho})C^{*}_{\mathbf{k}'+\rho-\delta}\Big)\Big)\\
&-\Big[\frac{e\hbar}{2m}\sum_{\mathbf{q},\delta,\gamma}(2(\mathbf{k}'-\mathbf{q}+\rho-\delta)+\mathbf{q})A_{\mathbf{q}}\Big]\times\\
&\qquad\beta_{\mathbf{k}'+\rho}\Big(m_{\mathbf{k}',\gamma}\Big((m^{*}_{\mathbf{k}'+\rho-\delta-q,\gamma+\delta+q-\rho}m_{\mathbf{k}'+\rho-\delta,\delta}+n_{\mathbf{k}'+\rho-\delta-q,\gamma+\delta+q-\rho}n^{*}_{\mathbf{k}'+\rho-\delta,\delta})L^{+}_{\mathbf{k}'-\mathbf{q}+\rho-\delta,\mathbf{q}}\\
&\qquad\qquad+(-m_{\mathbf{k}'+\rho-\delta,\delta}n_{\mathbf{k}'+\rho-\delta-q,\gamma+\delta+q-\rho}+n^{*}_{\mathbf{k}'+\rho-\delta,\delta}m^{*}_{\mathbf{k}'+\rho-\delta-q,\gamma+\delta+q-\rho})M^{-}_{\mathbf{k}'-\mathbf{q}+\rho-\delta,\mathbf{q}}\Big)\\
&\qquad+l_{\mathbf{k}',\gamma}\Big((m_{\mathbf{k}'+\rho-\delta,\delta}l^{*}_{\mathbf{k}'+\rho-\delta-q,\gamma+\delta+q-\rho}+n^{*}_{\mathbf{k}'+\rho-\delta,\delta}o_{\mathbf{k}'+\rho-\delta-q,\gamma+\delta+q-\rho})L^{+}_{\mathbf{k}'-\mathbf{q}+\rho-\delta,\mathbf{q}}\\
&\qquad\qquad+(-m_{\mathbf{k}'+\rho-\delta,\delta}o_{\mathbf{k}'+\rho-\delta-q,\gamma+\delta+q-\rho}+n^{*}_{\mathbf{k}'+\rho-\delta,\delta}l^{*}_{\mathbf{k}'+\rho-\delta-q,\gamma+\delta+q-\rho})M^{-}_{\mathbf{k}'-\mathbf{q}+\rho-\delta,\mathbf{q}}\Big)\Big)\\
&-\Big[\frac{e^{2}}{2m}\sum_{\mathbf{q},\delta,\gamma}\Big(\sum_{\mathbf{q}'}A_{\mathbf{q}-\mathbf{q}'}\cdot A_{\mathbf{q}'}\Big)\Big]\times\\
&\qquad\beta_{\mathbf{k}'+\rho}\Big(m_{\mathbf{k}',\gamma}\Big((m^{*}_{\mathbf{k}'+\rho-\delta-q,\gamma+\delta+q-\rho}m_{\mathbf{k}'+\rho-\delta,\delta}-n_{\mathbf{k}'+\rho-\delta-q,\gamma+\delta+q-\rho}n^{*}_{\mathbf{k}'+\rho-\delta,\delta})L^{-}_{\mathbf{k}'-\mathbf{q}+\rho-\delta,\mathbf{q}}\\
&\qquad\qquad-(m_{\mathbf{k}'+\rho-\delta,\delta}n_{\mathbf{k}'+\rho-\delta-q,\gamma+\delta+q-\rho}+n^{*}_{\mathbf{k}'+\rho-\delta,\delta}m^{*}_{\mathbf{k}'+\rho-\delta-q,\gamma+\delta+q-\rho})M^{+}_{\mathbf{k}'-\mathbf{q}+\rho-\delta,\mathbf{q}}\Big)\\
&\qquad+l_{\mathbf{k}',\gamma}\Big((m_{\mathbf{k}'+\rho-\delta,\delta}l^{*}_{\mathbf{k}'+\rho-\delta-q,\gamma+\delta+q-\rho}-n^{*}_{\mathbf{k}'+\rho-\delta,\delta}o_{\mathbf{k}'+\rho-\delta-q,\gamma+\delta+q-\rho})L^{-}_{\mathbf{k}'-\mathbf{q}+\rho-\delta,\mathbf{q}}\\
&\qquad\qquad-(m_{\mathbf{k}'+\rho-\delta,\delta}o_{\mathbf{k}'+\rho-\delta-q,\gamma+\delta+q-\rho}+n^{*}_{\mathbf{k}'+\rho-\delta,\delta}l^{*}_{\mathbf{k}'+\rho-\delta-q,\gamma+\delta+q-\rho})M^{+}_{\mathbf{k}'-\mathbf{q}+\rho-\delta,\mathbf{q}}\Big)\Big)
\end{aligned}
\tag{A.4}
$$

For $\alpha_{\mathbf{k}'}$ we collect like terms by choosing $\mathbf{k}' + \rho = \mathbf{k} + \eta$:

$$
\begin{aligned}
&i\hbar\frac{d}{dt}o_{\mathbf{k}',\rho}(t)\alpha_{\mathbf{k}'+\rho} = \\
&\sum_{\eta,\gamma}\alpha_{\mathbf{k}'+\rho}\Big(o_{\mathbf{k}',\gamma}\Big((l_{\mathbf{k}'+\rho-\eta,\gamma+\eta-\rho}l^*_{\mathbf{k}'+\rho-\eta,\eta} - o^*_{\mathbf{k}'+\rho-\eta,\gamma+\eta-\rho}o_{\mathbf{k}'+\rho-\eta,\eta})R_{\mathbf{k}'+\rho-\eta} \\
&\qquad\qquad + (l_{\mathbf{k}'+\rho-\eta,\gamma+\eta-\rho}o_{\mathbf{k}'+\rho-\eta,\eta})C_{\mathbf{k}'+\rho-\eta} + (l^*_{\mathbf{k}'+\rho-\eta,\eta}o^*_{\mathbf{k}'+\rho-\eta,\gamma+\eta-\rho})C^*_{\mathbf{k}'+\rho-\eta}\Big) \\
&\quad + n_{\mathbf{k}',\gamma}\Big((m_{\mathbf{k}'+\rho-\eta,\gamma+\eta-\rho}l^*_{\mathbf{k}'+\rho-\eta,\eta} - n^*_{\mathbf{k}'+\rho-\eta,\gamma+\eta-\rho}o_{\mathbf{k}'+\rho-\eta,\eta})R_{\mathbf{k}'+\rho-\eta} \\
&\qquad\qquad + (m_{\mathbf{k}'+\rho-\eta,\gamma+\eta-\rho}o_{\mathbf{k}'+\rho-\eta,\eta})C_{\mathbf{k}'+\rho-\eta} + (l^*_{\mathbf{k}'+\rho-\eta,\eta}n^*_{\mathbf{k}'+\rho-\eta,\gamma+\eta-\rho})C^*_{\mathbf{k}'+\rho-\eta}\Big)\Big) \\
&+ \Big[\frac{e\hbar}{2m}\sum_{\mathbf{q},\eta,\gamma}(2(\mathbf{k}'+\rho-\eta)+\mathbf{q})A_{\mathbf{q}}\Big]\times \\
&\quad \alpha_{\mathbf{k}'+\rho}\Big(o_{\mathbf{k}',\gamma}\Big((l_{\mathbf{k}'+\rho-\eta+q,\gamma+\eta-q-\rho}l^*_{\mathbf{k}'+\rho-\eta,\eta} + o^*_{\mathbf{k}'+\rho-\eta+q,\gamma+\eta-q-\rho}o_{\mathbf{k}'+\rho-\eta,\eta})L^+_{\mathbf{k}'+\rho-\eta,\mathbf{q}} \\
&\qquad\qquad + (-l_{\mathbf{k}'+\rho-\eta+q,\gamma+\eta-q-\rho}o_{\mathbf{k}'+\rho-\eta,\eta} + l^*_{\mathbf{k}'+\rho-\eta,\eta}o^*_{\mathbf{k}'+\rho-\eta+q,\gamma+\eta-q-\rho})M^-_{\mathbf{k}'+\rho-\eta,\mathbf{q}}\Big) \\
&\quad + n_{\mathbf{k}',\gamma}\Big((m_{\mathbf{k}'+\rho-\eta+q,\gamma+\eta-q-\rho}l^*_{\mathbf{k}'+\rho-\eta,\eta} + n^*_{\mathbf{k}'+\rho-\eta+q,\gamma+\eta-q-\rho}o_{\mathbf{k}'+\rho-\eta,\eta})L^+_{\mathbf{k}'+\rho-\eta,\mathbf{q}} \\
&\qquad\qquad + (-m_{\mathbf{k}'+\rho-\eta+q,\gamma+\eta-q-\rho}o_{\mathbf{k}'+\rho-\eta,\eta} + n^*_{\mathbf{k}'+\rho-\eta+q,\gamma+\eta-q-\rho}l^*_{\mathbf{k}'+\rho-\eta,\eta})M^-_{\mathbf{k}'+\rho-\eta,\mathbf{q}}\Big)\Big) \\
&+ \Big[\frac{e^2}{2m}\sum_{\mathbf{q},\eta,\gamma}\Big(\sum_{\mathbf{q}'}A_{\mathbf{q}-\mathbf{q}'}\cdot A_{\mathbf{q}'}\Big)\Big]\times \\
&\quad \alpha_{\mathbf{k}'+\rho}\Big(o_{\mathbf{k}',\gamma}\Big((l_{\mathbf{k}'+\rho-\eta+q,\gamma+\eta-q-\rho}l^*_{\mathbf{k}'+\rho-\eta,\eta} - o^*_{\mathbf{k}'+\rho-\eta+q,\gamma+\eta-q-\rho}o_{\mathbf{k}'+\rho-\eta,\eta})L^-_{\mathbf{k}'+\rho-\eta,\mathbf{q}} \\
&\qquad\qquad - (l_{\mathbf{k}'+\rho-\eta+q,\gamma+\eta-q-\rho}o_{\mathbf{k}'+\rho-\eta,\eta} + l^*_{\mathbf{k}'+\rho-\eta,\eta}o^*_{\mathbf{k}'+\rho-\eta+q,\gamma+\eta-q-\rho})M^+_{\mathbf{k}'+\rho-\eta,\mathbf{q}}\Big) \\
&\quad + n_{\mathbf{k}',\gamma}\Big((m_{\mathbf{k}'+\rho-\eta+q,\gamma+\eta-q-\rho}l^*_{\mathbf{k}'+\rho-\eta,\eta} - n^*_{\mathbf{k}'+\rho-\eta+q,\gamma+\eta-q-\rho}o_{\mathbf{k}'+\rho-\eta,\eta})L^-_{\mathbf{k}'+\rho-\eta,\mathbf{q}} \\
&\qquad\qquad - (m_{\mathbf{k}'+\rho-\eta+q,\gamma+\eta-q-\rho}o_{\mathbf{k}'+\rho-\eta,\eta} + n^*_{\mathbf{k}'+\rho-\eta+q,\gamma+\eta-q-\rho}l^*_{\mathbf{k}'+\rho-\eta,\eta})M^+_{\mathbf{k}'+\rho-\eta,\mathbf{q}}\Big)\Big)
\end{aligned}
\tag{A.5}
$$

and for $\beta^\dagger_{\mathbf{k}'}$, $\mathbf{k}'+\rho=\mathbf{k}+\eta$:

$$
\begin{aligned}
&i\hbar\frac{d}{dt}n_{\mathbf{k}',\rho}(t)\beta^\dagger_{\mathbf{k}'+\rho}=\\
&\sum_{\eta,\gamma}\beta^\dagger_{\mathbf{k}'+\rho}\Big(n_{\mathbf{k}',\gamma}\Big((m^*_{\mathbf{k}'+\rho-\eta,\eta}m_{\mathbf{k}'+\rho-\eta,\gamma+\eta-\rho}-n_{\mathbf{k}'+\rho-\eta,\eta}n^*_{\mathbf{k}'+\rho-\eta,\gamma+\eta-\rho})R_{\mathbf{k}'+\rho-\eta}\\
&\qquad\qquad+(m_{\mathbf{k}'+\rho-\eta,\gamma+\eta-\rho}n_{\mathbf{k}'+\rho-\eta,\eta})C_{\mathbf{k}'+\rho-\eta}+(m^*_{\mathbf{k}'+\rho-\eta,\eta}n^*_{\mathbf{k}'+\rho-\eta,\gamma+\eta-\rho})C^*_{\mathbf{k}'+\rho-\eta}\Big)\\
&\qquad+o_{\mathbf{k}',\gamma}\Big((l_{\mathbf{k}'+\rho-\eta,\gamma+\eta-\rho}m^*_{\mathbf{k}'+\rho-\eta,\eta}-n_{\mathbf{k}'+\rho-\eta,\eta}o^*_{\mathbf{k}'+\rho-\eta,\gamma+\eta-\rho})R_{\mathbf{k}'+\rho-\eta}\\
&\qquad\qquad+(l_{\mathbf{k}'+\rho-\eta,\gamma+\eta-\rho}n_{\mathbf{k}'+\rho-\eta,\eta})C_{\mathbf{k}'+\rho-\eta}+(o^*_{\mathbf{k}'+\rho-\eta,\gamma+\eta-\rho}m^*_{\mathbf{k}'+\rho-\eta,\eta})C^*_{\mathbf{k}'+\rho-\eta}\Big)\Big)\\
&+\Big[\frac{e\hbar}{2m}\sum_{\mathbf{q},\eta,\gamma}(2(\mathbf{k}'+\rho-\eta)+\mathbf{q})A_{\mathbf{q}}\Big]\times\\
&\quad\beta^\dagger_{\mathbf{k}'+\rho}\Big(n_{\mathbf{k}',\gamma}\Big((m^*_{\mathbf{k}'+\rho-\eta,\eta}m_{\mathbf{k}'+\rho-\eta+q,\gamma+\eta-q-\rho}n_{\mathbf{k}'+\rho-\eta,\eta}+n^*_{\mathbf{k}'+\rho-\eta+q,\gamma+\eta-q-\rho})L^+_{\mathbf{k}'+\rho-\eta,\mathbf{q}}\\
&\qquad\qquad+(-m_{\mathbf{k}'+\rho-\eta+q,\gamma+\eta-q-\rho}n_{\mathbf{k}'+\rho-\eta,\eta}+n^*_{\mathbf{k}'+\rho-\eta+q,\gamma+\eta-q-\rho}m^*_{\mathbf{k}'+\rho-\eta,\eta})M^-_{\mathbf{k}'+\rho-\eta,\mathbf{q}}\Big)\\
&\qquad+o_{\mathbf{k}',\gamma}\Big((l_{\mathbf{k}'+\rho-\eta+q,\gamma+\eta-q-\rho}m^*_{\mathbf{k}'+\rho-\eta,\eta}+n_{\mathbf{k}'+\rho-\eta,\eta}o^*_{\mathbf{k}'+\rho-\eta+q,\gamma+\eta-q-\rho})L^+_{\mathbf{k}'+\rho-\eta,\mathbf{q}}\\
&\qquad\qquad+(-l_{\mathbf{k}'+\rho-\eta+q,\gamma+\eta-q-\rho}n_{\mathbf{k}'+\rho-\eta,\eta}+o^*_{\mathbf{k}'+\rho-\eta+q,\gamma+\eta-q-\rho}m^*_{\mathbf{k}'+\rho-\eta,\eta})M^-_{\mathbf{k}'+\rho-\eta,\mathbf{q}}\Big)\Big)\\
&+\Big[\frac{e^2}{2m}\sum_{\mathbf{q},\eta,\gamma}\Big(\sum_{\mathbf{q}'}A_{\mathbf{q}-\mathbf{q}'}\cdot A_{\mathbf{q}'}\Big)\Big]\times\\
&\quad\beta^\dagger_{\mathbf{k}'+\rho}\Big(n_{\mathbf{k}',\gamma}\Big((m^*_{\mathbf{k}'+\rho-\eta,\eta}m_{\mathbf{k}'+\rho-\eta+q,\gamma+\eta-q-\rho}-n_{\mathbf{k}'+\rho-\eta,\eta}n^*_{\mathbf{k}'+\rho-\eta+q,\gamma+\eta-q-\rho})L^-_{\mathbf{k}'+\rho-\eta,\mathbf{q}}\\
&\qquad\qquad-(m_{\mathbf{k}'+\rho-\eta+q,\gamma+\eta-q-\rho}n_{\mathbf{k}'+\rho-\eta,\eta}+n^*_{\mathbf{k}'+\rho-\eta+q,\gamma+\eta-q-\rho}m^*_{\mathbf{k}'+\rho-\eta,\eta})M^+_{\mathbf{k}'+\rho-\eta,\mathbf{q}}\Big)\\
&\qquad+o_{\mathbf{k}',\gamma}\Big((l_{\mathbf{k}'+\rho-\eta+q,\gamma+\eta-q-\rho}m^*_{\mathbf{k}'+\rho-\eta,\eta}-n_{\mathbf{k}'+\rho-\eta,\eta}o^*_{\mathbf{k}'+\rho-\eta+q,\gamma+\eta-q-\rho})L^-_{\mathbf{k}'+\rho-\eta,\mathbf{q}}\\
&\qquad\qquad-(l_{\mathbf{k}'+\rho-\eta+q,\gamma+\eta-q-\rho}n_{\mathbf{k}'+\rho-\eta,\eta}+o^*_{\mathbf{k}'+\rho-\eta+q,\gamma+\eta-q-\rho}m^*_{\mathbf{k}'+\rho-\eta,\eta})M^+_{\mathbf{k}'+\rho-\eta,\mathbf{q}}\Big)\Big)
\end{aligned}
\tag{A.6}
$$